The Report Committee for Inyeop Jung
Certifies that this is the approved version of the following report:

Geometric Location and Power Distribution for Discrete Heat Sources on a Vertical Flat Plate with Natural Convection

APPROVED BY

SUPERVISING COMMITTEE:

Supervisor:

Alexandre K. da Silva

John R. Howell

Geometric Location and Power Distribution for Discrete Heat Sources on a Vertical Flat Plate with Natural Convection

by

Inyeop Jung, BSME

Report

Presented to the Faculty of the Graduate School of

The University of Texas at Austin

in Partial Fulfillment

of the Requirements

for the Degree of

Master of Science in Engineering

The University of Texas at Austin

August 2011

Dedication

To my beloved family—without your endless support and love, nine years of studying abroad in the states would not have been possible

Acknowledgements

I would like to say how thankful I am to have very dedicated and passionate Professor Alexandre K. da Silva as my research supervisor. His knowledge and insight on the subject matter has broadened my eyes to not only the research subject, but also other aspects of working in the lab. He has taken me as an Undergraduate Research Assistant in Fall semester of 2008, giving me great opportunity to get hands-on experience. Since then, he helped me not only with the research, but also numerous things that regarding school and much more. It was an absolute pleasure getting to know a professor who cares about his student as much as Professor da Silva. Without his help and knowledge, the completion of the research project wouldn't have been possible.

I would also like to thank Professor John R. Howell, the report committee member, for taking his time and effort to review this report. Taking a class from one of the most distinguished scholars in radiation heat transfer area in the Spring of 2010 helped me gain knowledge about radiative heat transfer. It was a great joy and very enlightening to learn from him.

Also, without the Dr. David G. Bogard's exceptional knowledge in the experimental research, the accurate surface temperature measurement would not have been possible. His input and insight helped greatly in the improvement of the test sections and its measurement techniques.

Last but not least, I would like to thank Robert Hart. His knowledge from vast amount of experimental research has helped me with measurement techniques and troubleshooting problems over the course of the project. Working with him in the lab was very valuable and pleasurable experience for me.

Abstract

Geometric Location and Power Distribution for Discrete Heat Sources on a Vertical Flat Plate with Natural Convection

Inyeop Jung, MSE

The University of Texas at Austin, 2011

Supervisor: Alexandre K. da Silva

The current development of consumer electronics, driven by the effort to manufacture smaller products with increased performance, has amplified the chance for inducing higher thermal stresses to these systems. In an effort to devise more effective cooling methods for these systems, many scholars have studied the convective cooling of discrete heating elements.

This report discusses a methodology for fabricating and testing a suitable flat plate design with discrete heating elements for both natural and forced convection cooling experiments. There were two plate design attempts: (i) an aluminum plate and (ii) a R3315 hydrostatic-resistance plastic foam plate. For the purpose of conducting experiments for the discrete heating elements, the foam plate design was found to be an appropriate design.

After designing a proper foam plate, several experiments were conducted for the natural convection case. The combination of parameters such as the geometric location and power output ratio between heaters that resulted in the maximum thermal conductance were studied.

Table of Contents

List of Tables

List of Figures

Chapter 1 Introduction

1.1 Motivation

With development of electronic components, engineers have been able to reduce the size of consumer's electronics considerably while improving their performances. Lighter, thinner, and more portable laptop computers are merging into the market faster than anyone can imagine; Liquid Crystal Display High Definition televisions, which replaced bulky plasma televisions, are now being replaced by ultra thin Light Emitting Diode High Definition televisions; the so-called smart phones are like small computer in a palm of one's hand [1, 2].

Making the consumer electronics smaller, while improving the performances, is the goal that engineers are trying to achieve. However, such trend poses technical problems—higher performance represents higher heat generation, and smaller size means less space to dissipate the generated heat. For instance, if efficient cooling is not achieved, thermal stresses may result in malfunctioning electronic components and may even cause the failure of the entire system if these are imposed for extended periods [3]. There are several ways of approaching the problem, such as to design more effective cooling systems, changing materials, and design modifications are some of the options available.

If the cooling methods of a system were to be improved, there are several different options that one can consider, such as forced, natural and mixed convection. Forced convection is one of the most used cooling methods for electronic components with very high heat generation rates, such as computers, laptops, gaming consoles and DVD players. Natural convection, however, is generally used in the electronic products

with larger surface area and relatively less heat generation, such as televisions and LCD monitors.

1.2 Literature Review

Many scholars have acknowledged the problem over the years and have tried to present solutions to increase cooling performances. There are many numerical works on cooling of discrete heaters, which represent electrical components, using forced, natural and mixed convection methods with different geometries and placement of heaters.

The numerical studies of forced convection with different geometries were investigated by many scholars. The most common geometry is the flat plate; References [4-6] are some of the examples of forced convection cooling on a flat plate with discrete heaters. Other geometries, such as cavity [7], inclined wall [8], and even a flow in a porous media [9] were also studied.

Many of the numerical works on natural convection are also done with flat plate, or in an open channel [10-12]. Some studied the effect of having the discrete heat sources in various geometry, such as open cavity [13, 14], and rectangular enclosures, [15]. Mixed cooling also was under the microscope of scholars trying to study the effect of discrete heat sources. There are several numerical studies done on a flat plate with open channel with discrete heaters [7, 16, 17].

Cooling method and geometry were not the only variables considered in these studies. The power dissipation ratios, number of discrete heaters, location of heaters, and flow velocity were also varied. For example, Refs. [5] and [6] investigated the effect of forced convection cooling on a flat plate, while using different variables. For instance,

Ref. [5] fixes the heat source strength and varies the fluid flow velocity, whereas in Ref. [6], the pressure driven flow remains as constant and the heat source strength is varied. Also, Refs. [10] and [12] discussed the optimal distribution of discrete heat sources in natural convection on a flat plate.

It was not only numerical works that were done to study the cooling effect on the discrete heaters, but some experimental studies also considered the problem. As the flat plate was the most popular choice in the numerical studies, most of the experimental studies also chose flat plate in either natural or forced convection (e.g., [13, 18-20]). Most of these studies mentioned the "thermal conductance" as the variable of interest, which measures how well the heat is being transferred to the working fluid. If the thermal conductance value is higher, lower maximal temperature is expected.

1.3 Proposed Work

This study presents the methodology for fabricating two test sections for cooling discrete heat sources in natural and forced convection. Experimental tests focused on the study of natural convection with a vertical plate configuration. The experiments were performed by varying the location and power dissipation ratios between the heaters. From the sets of experiments, the optimal combination of these variables resulting in the maximum thermal conductance was found.

In Chapter 2, the design and fabrication of the wind tunnel core section, types of heaters used, two plate designs and their materials (i.e., Aluminum and R3315 hydrostatic-pressure resistance foam), and the assembling procedure are discussed. Numerous figures are presented to help the readers understand the experimental setup.

Chapter 3 will discuss the proposed experimental setup for both natural and forced convection tests. The design and assembly processes of the wind tunnel for the forced convection are explained, and the natural convection experimental setup also is discussed in this chapter.

Chapter 4 discusses the experimental methodology. This chapter includes fluid flow velocity and temperature measurement methods for forced convection. In addition, the temperature measurement setup with thermocouples and an infrared camera for natural convection experiment is also presented. Furthermore, a detailed explanation about the issues with the aluminum plate design and why it was not considered a practical test section for the purpose of the presented study is provided.

The following chapter, Chapter 5, the experimental procedure for natural convection tests with discrete heaters is explained. These tests were aimed to achieve the maximum thermal conductance by changing power dissipation ratios between the heaters and the location of heaters while the total wattage was fixed. The fixed total wattage was also changed to study the effect of different total power dissipation rates.

Chapter 6 discusses the experimental data and the results obtained. The measured data was presented to show the effect of having different geometric locations and power dissipation ratios between the heaters. From the obtained data, thermal conductance was calculated and graphed to illustrate the effect of changing variables.

The last chapter, Chapter 7, will recapitulate the presented information, and the suggestions for future work entailing this research will be discussed.

Chapter 2 Discretely Heated Plate Designs and Assembly

Two attempts to design a suitable plate for testing the cooling effect on discrete heating elements were made: (i) aluminum plate design, (ii) foam plate design. For the reasons explained in subchapter 4.1.2, the first design using the aluminum sheets was regarded as improper, and new plate material and design methodology were created. With the second design, sufficient insulation between the discrete heaters is achieved, allowing better results. In this chapter, the details about both plates will be discussed.

2.1 Aluminum Plate

2.1.1 Plate Design

The first plate design used two 6061 Temper O aluminum sheets, with thermal conductivity of 166 [W/m·K]. The thickness of each sheet was 0.079 inches and the leading edge was designed with an ellipse shape—the ratio between the major axis of the plate leading edge was 25 to 1. This ensured a very sharp leading edge that would not disturb the entrance fluid to the plate, i.e., a smooth start of the boundary layer. The installed test plate was an assembly of two identical halves. Since each side of the plate was a single piece of aluminum sheet, 2.000 mm wide by 1.000 mm deep grooves, perpendicular to the fluid flow direction were cut every 0.500 inches in the inner surfaces of both plates to limit axial conduction along the aluminum piece. This also served as a space for thermocouples to be installed. The entire plate was designed to accommodate 28 discrete heaters and was 452 mm long. The dimensions of the aluminum plate are given in Figure 2-1.

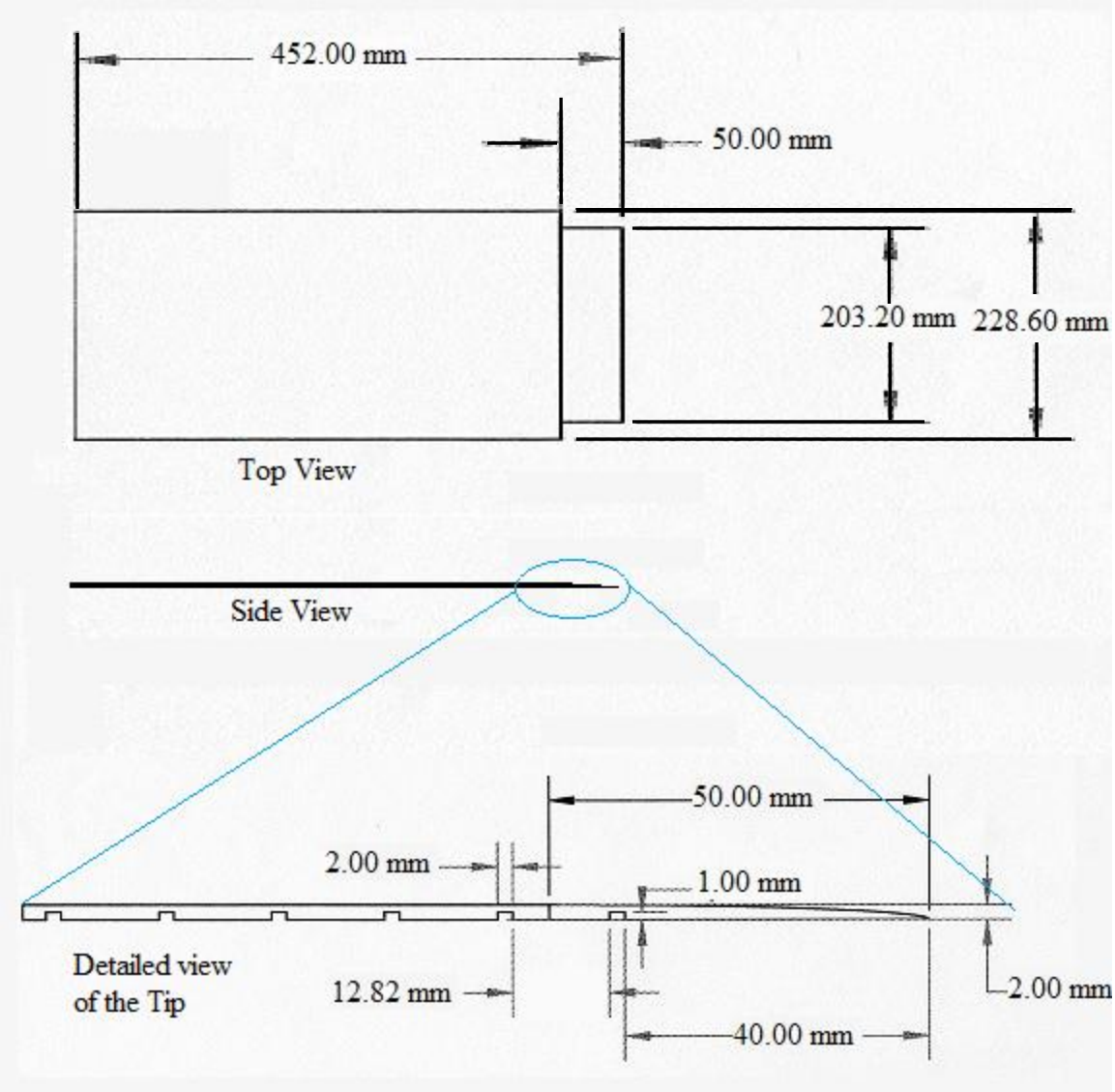

Figure 2-1 Dimensions of the aluminum plate design

2.1.2 Heating Elements

The heating element used for the aluminum plate design was a thin ribbon type bare heating wire from Omega Engineering, Inc. The width and thickness of the heating element were 1/64 × 0.002 inches respectively [21]. The spool of ribbon wire was cut to the length extending 0.500 inch beyond the aluminum plate for the electrical connections

to the power supply. The wire was composed of Nickel-Chromium Alloy, 60% Nickel/16% Chromium, and balance iron [21].

2.1.3 Plate Assembly

On the inner side of the aluminum plate, the first layer of Kapton® tape was adhered to the aluminum plate where the heating element would be laid. Then a strip of ribbon resistance wire was laid, on top of the first layer of Kapton® tape. On top of the heating wire, another layer of Kapton® tape was applied to secure the heating wire in place (shown in Figure 2-2). The ends of the ribbon wires are extended beyond the aluminum plate for electrical connection. Due to its geometry, being the ribbon type wire, it was difficult to connect each resistance wires to the electrical connection posts. Therefore, a normal 18 American Wire Gage (AWG) electrical wire was welded to the ends of the ribbon wires, and was wrapped with heat shrinking tubes for the insulation and safety reasons.

After installing the heating elements, K-type thermocouples with bid tips were placed in the machined grooves of the aluminum plate for the temperature measurements. The tips of the thermocouples were facing towards the inner surface of the aluminum plate, and were insulated by a small piece of Kapton® tape (see Figure 2-2).

The second piece of the aluminum plate in identical dimensions was put together, and this assembly was fitted into the cutouts on the sidewalls of the wind tunnel test section that is discussed in Chapter 3.1. The cutouts on the wind tunnel provided a very tight fit and this ensured that the two plates would not separate and the gap between the plates was completely shut.

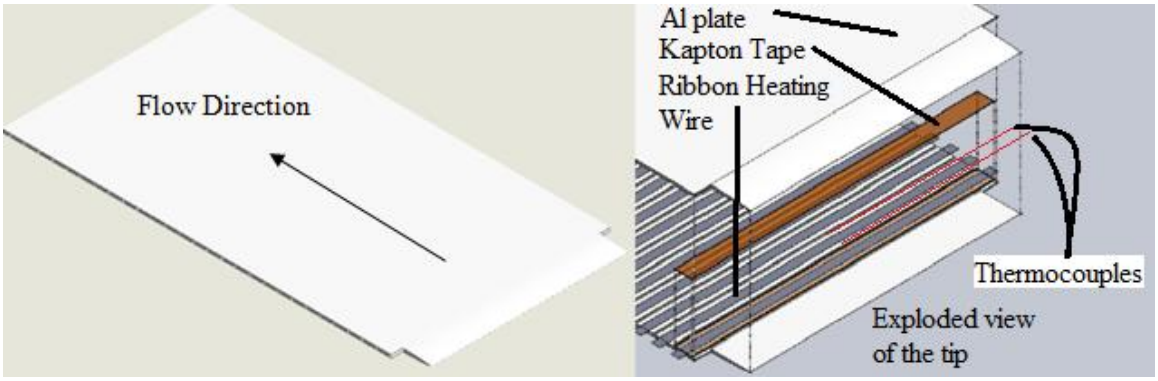

Figure 2-2 Aluminum plate design, heating element installation schematic drawing

The plate surfaces were painted with black spray paint, Krylon® Ultra Flat Camouflage Black, which has known emissivity of 0.98. The painted surface enabled the possibility of measuring the surface temperature with an infrared camera in the future.

2.2 R3315 Foam Plate

2.2.1 Plate Design

The second plate design used R3315 plastic foam from General Plastics Manufacturing Company as insulation between the heating elements [22]. The foam has thermal conductivity of 0.044 [W/m·K], which is very low compared to the thermal conductivity of the Al 6061 Temper O used in the previous design [22]. The general properties of the foam are attached in Appendix B.

This new insulation material minimized the conduction effects between the discrete heating elements. The ratio of the major axis of the ellipse of the leading edge was 5 to 1 for the foam plate, which was lower than that of the aluminum plate design. The total length of the foam was 13.667 inches and thickness of 0.500 inches. The foam plate design was thicker than the aluminum plate design due to the foam plate being too

brittle to be machined. The top and bottom surfaces of the plate had a total of 10 grooves, 2.000 × 8.000 × 0.070 inches in dimension, for each discrete heating element. The foam spacers to minimize the conduction effect between heaters were 0.333 inches. The dimensions and design of the foam plate are illustrated in Figure 2-3.

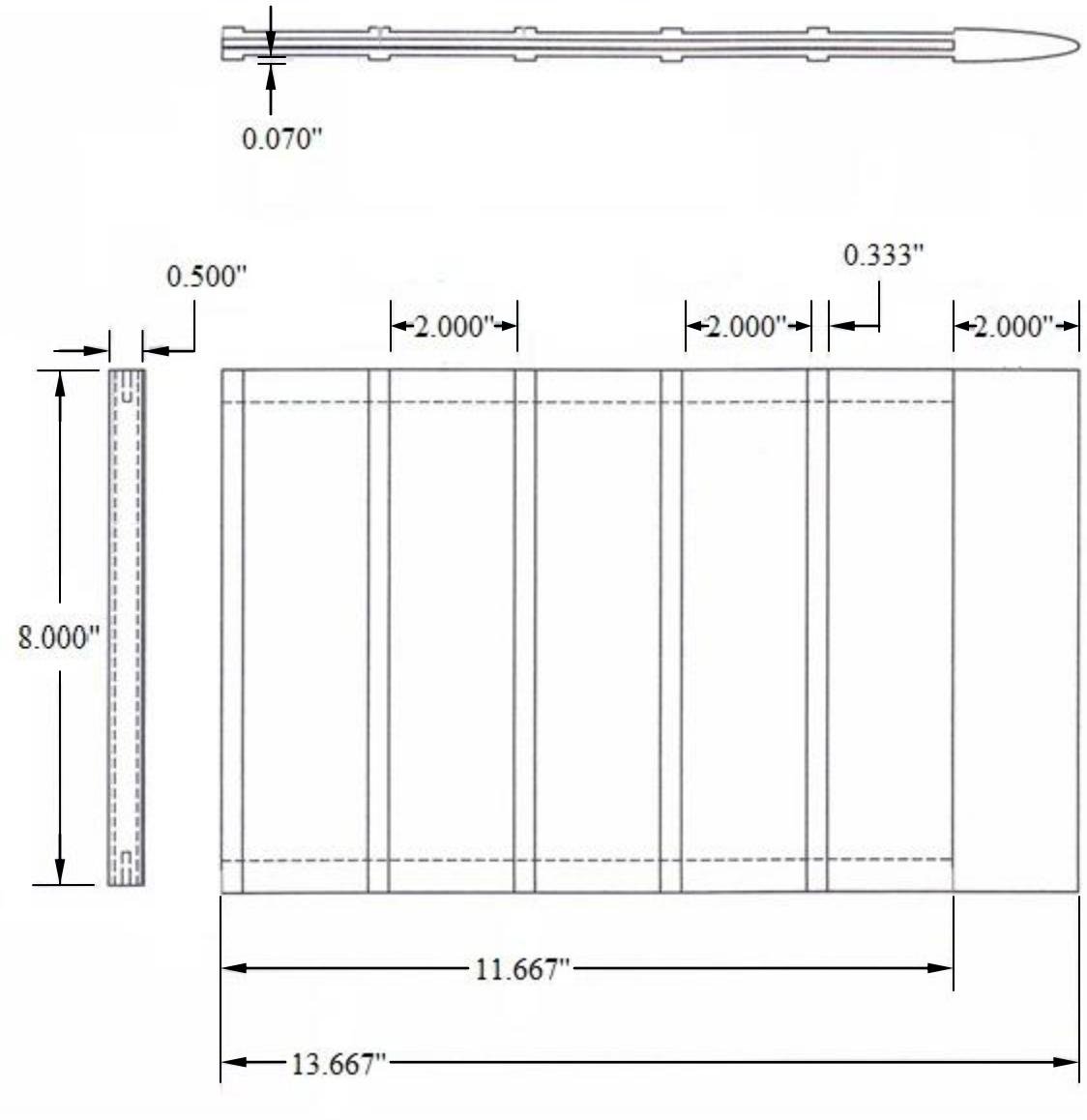

Figure 2-3 Dimensions of the R3315 Foam Plate

2.2.2 Heating Elements

10 Kapton® Heaters from Omega Engineering, Inc. were used as the constant heat flux supply. The heating element used had a watt density of 5 [W/in^2] [23]. The Kapton® Heater was made of a thin ribbon heating wire laid out in complex geometry between two layers of Kapton® material. Although the dimensions of the heating element were specified as 2×8 inches by the manufacturer, the actual heated surface was slightly smaller [23]. The reported dimensions of the Kapton® heater included insulating edges, approximately 3 to 4 mm of Kapton® material. This space caused the temperature of the aluminum plates with 2×8 inches in dimension that covered the Kapton® heater to simulate constant heat flux area, to dip near the edge. Each single heater had a nominal resistance of 156.78 ohms at the room temperature.

2.2.3 Plate Assembly

Each Kapton® Heater was adhered to a thin piece of Temper O 6061 aluminum plate, 2 $\times$ 8 inches in dimension, by applying thin layer of 5-minute epoxy. Between the heating element and the aluminum piece, three K-type thermocouples were installed along the centerline of the plate—at the front edge, middle of the plate, and at the back edge. This assembly was then secured to the foam using same 5-minute epoxy. The illustration of plate assembly and the dimensions of the plate are given in Figure 2-4.

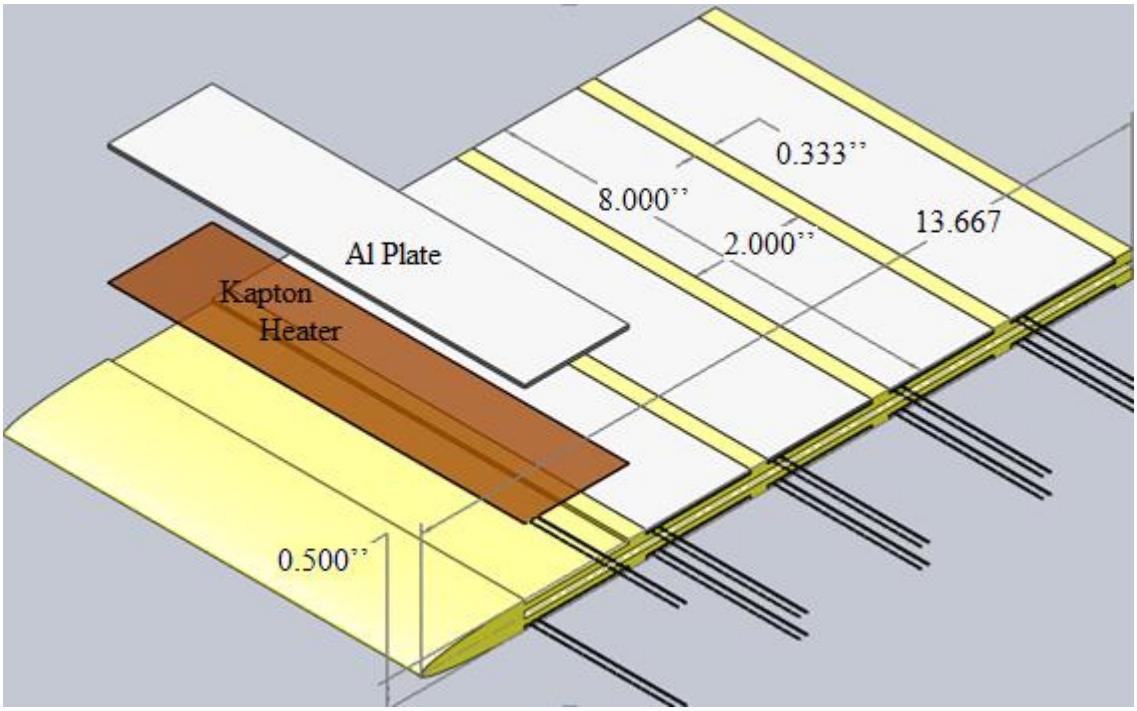

Figure 2-4 R3315 plate design, heating element installation illustration and dimensions

The grooves on the surfaces of R3315 foam were designed while accounting for the thickness of the aluminum and the Kapton® Heater assembly. However, the amount of epoxy and its final thickness were unknown at the time the plate was designed, so the grooves on the plate were cut slightly deeper than the calculated thickness of the heater assembly to accommodate the uncertainty of adhesive thickness. Therefore, once the heater assembly was adhered to the foam plate, the foam was ground away to match the height of plates. Although machined with low tolerances, the edges of the plate and the insulation areas appeared to show small gaps. To have an extra smooth surface, these gaps were filled with thermally conductive epoxy, with thermal conductivity 1.03 [W/m·K] [24]. The foam plate also was spray-painted black to have uniform radiation emissivity on the entire surface of the plate.

Chapter 3 Experimental Setup

The test section was designed based on an existing wind tunnel built by a former Mechanical Engineering student from The University of Texas at Austin. The existing wind tunnel parts, a honeycomb flow straightener, a flow expansion cone, and a 1 HP DC motor with Valdor motor controller were reused. The new test section was an assembly of machined 0.500 inch thick Polycarbonate pieces, which enabled a clear view of the test plate, and the fluid flow. The inner dimensions of the test section were 8.000 × 8.000 × 36.000 inches. The subchapter 3.1 will discuss the detailed dimensions and notable features of the newly designed test section assembly.

3.1 Forced Convection

The test section for forced convection assembly was composed of eight Polycarbonate pieces, which are labeled and shown in Figure 3-1: one 33.000 inch-long top piece (1), two 36.000 inch-long side walls (2-1, 2-2) , one 33.000 inch-long bottom piece (3), and four 1.500 inch-long pieces (4-1, 4-2, 4-3, 4-4). These four 1.500 inch-long pieces were used to close the gap that the top and bottom pieces created with the 36.000 inch-long side pieces. All of the Polycarbonate parts, except two 33.000 inch-long top and bottom, were fastened together using 1 inch long hex-head screws. The assembled Polycarbonate test section was attached to the two stainless steel brackets at each end with 0.500 inch-long hex-head screws. The test section design was taken from the previous wind tunnel test section, with modifications to accommodate the newly designed plates and other components, such as electrical connection posts and thermocouple connection blocks.

Top and bottom of the Polycarbonate pieces were only secured with 6 draw latches per piece. Although machined very precisely, a total of 16 dowel pins were used to hold the top and the bottom pieces to the sidewalls at the exact locations to ensure proper alignment. Using draw latches and dowel pins enabled the top and bottom pieces to be easily detached from the rest of the assembly for an easy access to the test plate. The exploded view of the test section assembly was shown in Figure 3-1. Once the test section was assembled, it was then attached to the rest of the wind tunnel body. The illustration of the wind tunnel is given in Figure 3-2.

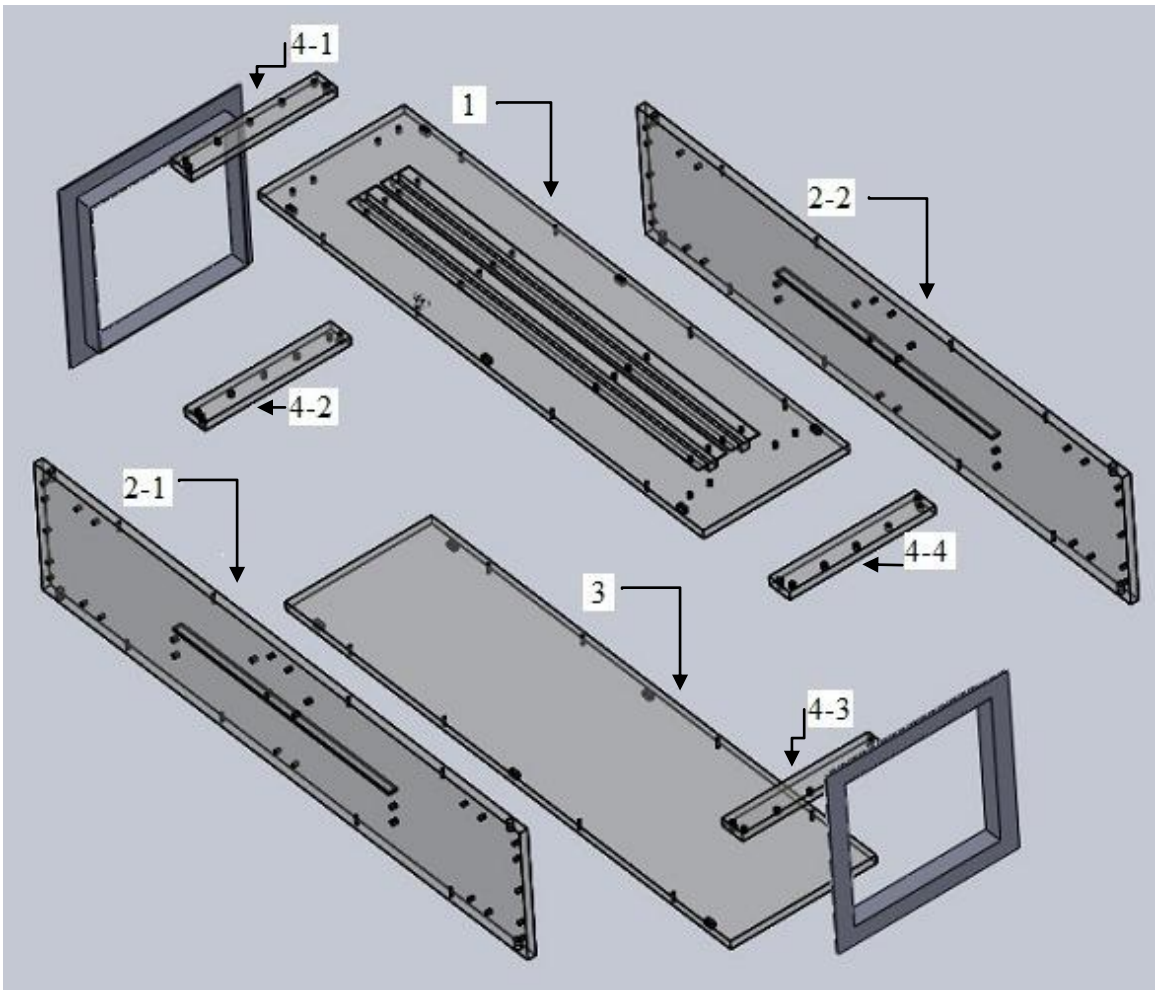

Figure 3-1 Exploded view of the wind tunnel test section assembly

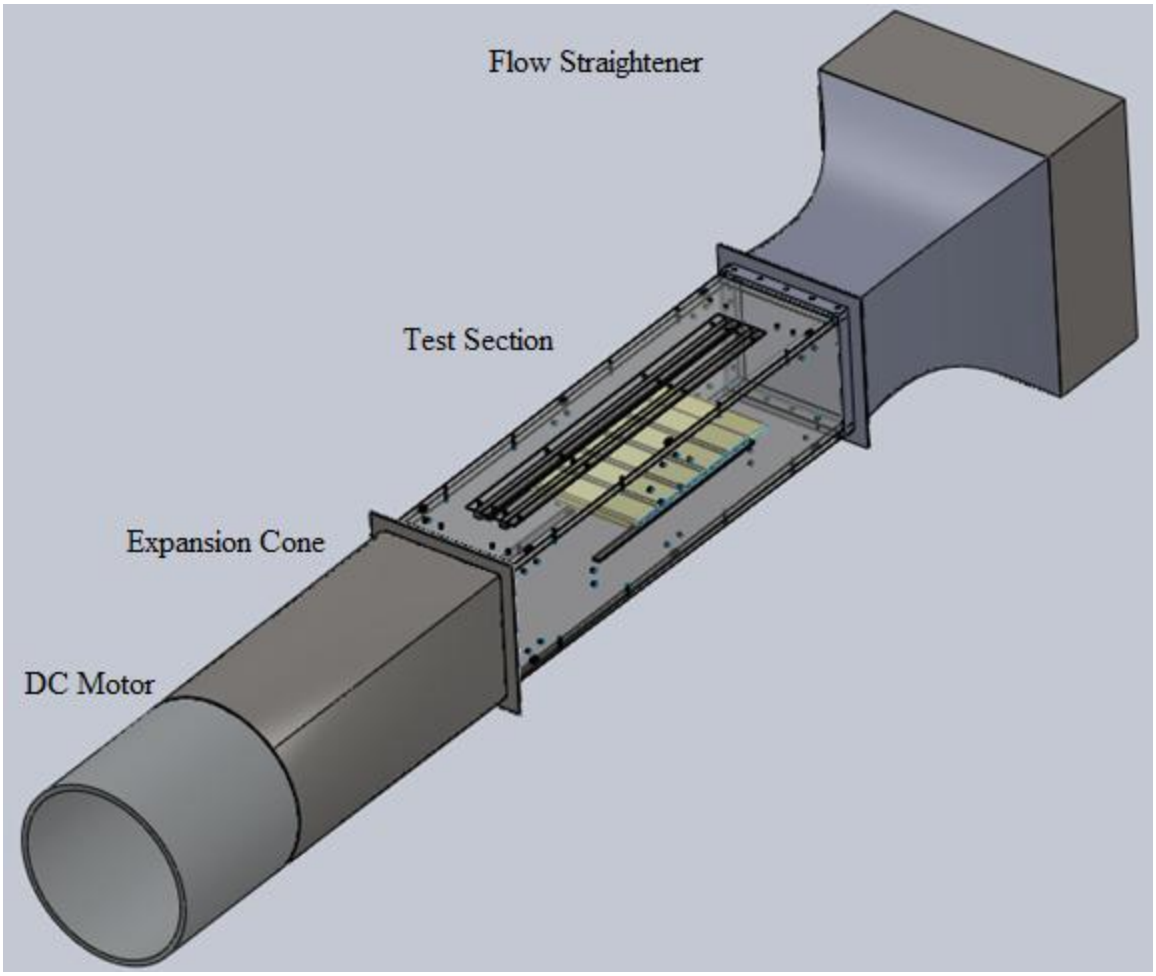

Figure 3-2 Schematic drawing of the entire wind tunnel for forced convection

The top Polycarbonate piece was 33.000 × 9.000 inches in dimension, with two rectangular shaped openings cut to allow a pitot-static tube and a thermocouple probe to be inserted and moved along the test section to measure characteristics of the fluid flow. The dimensions of these through extrusions are 0.500 × 26.000 inches and are separated from each other by 2.000 inches. The open spaces were covered with a metal-backed strip brushes to minimize air leakage from the test section to the surroundings. It also featured six 0.250 inch-deep extrusion cuts where the draw latches would hook into, and

eight through holes with 0.170 inches in diameter for dowel pin insertion near the edges. The bottom piece had the same overall length, width, and the machined features as the top piece, but the two rectangular through extrusion. The drawing of the top piece is given in Figure 3-3.

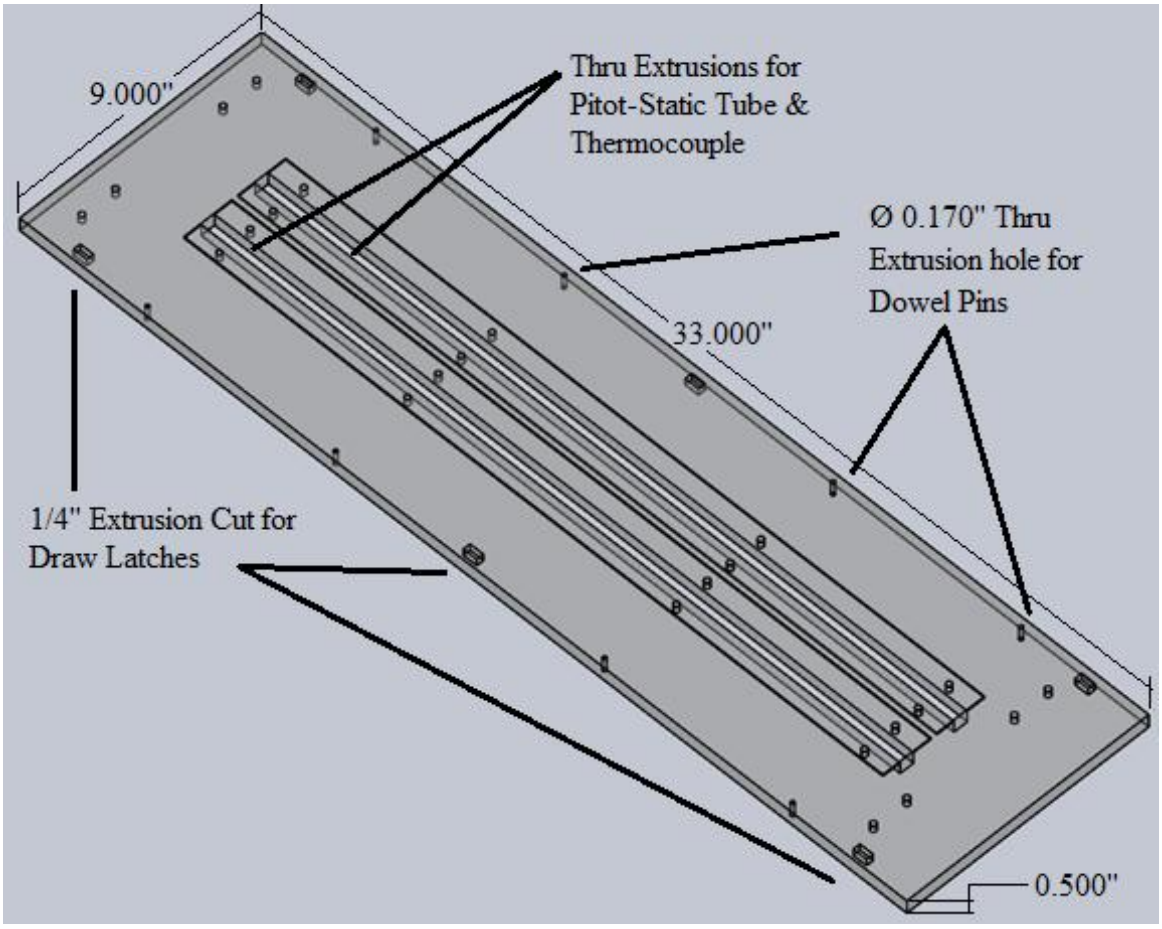

Figure 3-3 Wind tunnel test section, top piece- Isometric view

The two sidewalls of the test section pieces were measured at 36.000×8.000 inches. A thin through extrusion was machined at the centerline of both sidewalls—this feature held the test plate inside the test chamber. Other features include 0.250 inch-deep threaded extrusion holes for the installation of draw latches and electrical connections.

The two sides were identical in dimensions and features, except one sidewall had extra threaded holes for the attachment of the thermocouple connection panels.

After assembling the wind tunnel parts, the electrical and thermocouple connections were installed. For the electrical connections from the power supply to the heating elements, banana plug connectors were mounted onto the aluminum panel, and the assembly was fastened to each sidewalls. On the back side, miniature K-type thermocouple connection panels were installed to connect the thermocouple wires from the test piece to the digital data acquisition system, which would collect the data digitally.

3.2 Natural Convection

For the natural convection tests, the same wind tunnel assembly was used. The test section piece was disassembled from the wind tunnel body, then the top and the bottom Polycarbonate pieces were detached and the rest of the test section was set upright on a flat table. The leading edge was set towards the bottom so that the flow into the heated surfaces was less disturbed. The visual illustration of the natural convection test section is shown in Figure 3-4. The infrared camera was then installed approximately 60 cm away from the center of the plate, and the assembly shown in Figure 3-4 was surrounded with walls, which blocked all outer influences to the fluid flow near the foam plate.

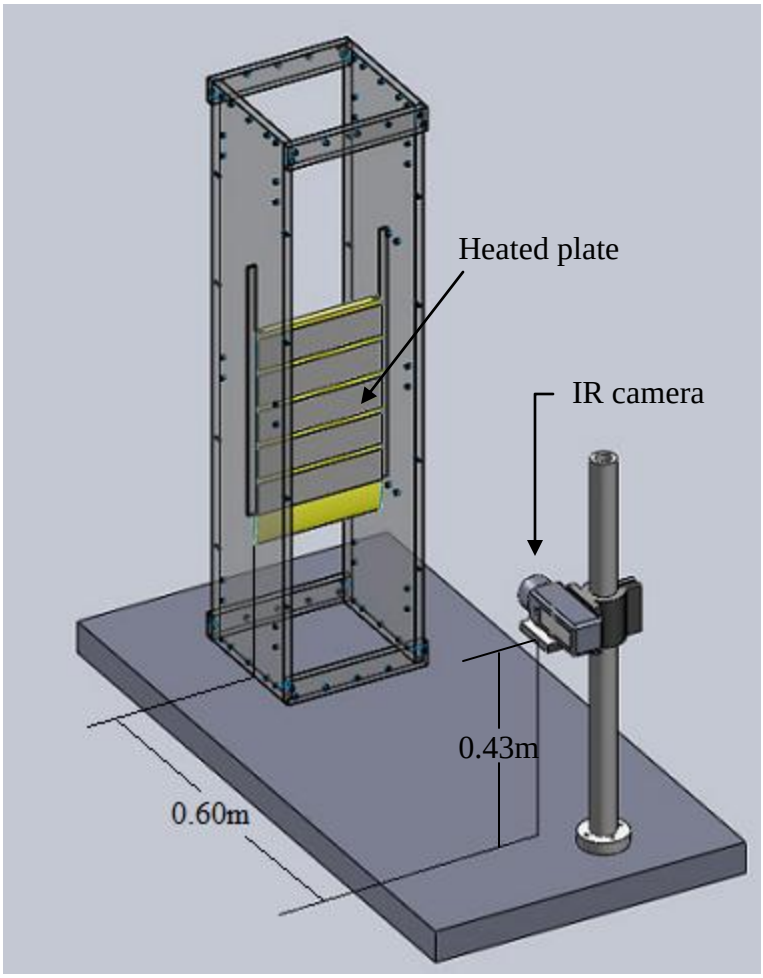

Figure 3-4 Schematic drawing of the natural convection test section setup. The surroundings were blocked to limit forced convection effect (Not shown).

Chapter 4 Experimental Methodology

In this chapter, a detailed discussion on the fluid flow measurements for forced convection and plate temperature readings for both natural and forced convection experiments were made. The calibration processes of temperature readings from an infrared camera and a thermocouple are also explained.

4.1 Forced Convection Measurements

4.1.1 Air Flow

For the forced convection experiments, a 1/8 inch stainless steel pitot-static tube from Dywer was used to measure the dynamic pressure of the air flow. The ends of the pitot-static tubes were connected to a digital manometer in order to measure and display the dynamic pressure inside the wind tunnel. With the obtained dynamic pressure value, one can find the velocity of fluid, using

$$P_{dynamic} = \frac{1}{2}\rho v^2 \qquad \text{(Eq. 4.1)}$$

where ρ is the density of air and v is the velocity of fluid [25].

As for the free stream temperature, a K-type thermocouple with bid tip was used. This thermocouple was set well ahead of the heating elements, so that the effects from the heated surfaces were negligible. The thermocouple and the pitot-static tube were both clamped onto a height gage sitting on the topside of the wind tunnel. The height gauge was resting on the top of two circular rods that were mounted on the top Polycarbonate piece, acting as the guiderail for the height gauge to move in the longitudinal direction. These rods and height gage enabled the pitot-static tube and the thermocouple to move in two axial direction easily. The temperature and the dynamic pressure were measured at

separate times. The free stream temperature was measured when the height gauge was set upstream of the plate, while the dynamic pressure was measured above the plate.

4.1.2 Plate Temperature Measurements

To obtain and record the temperatures of the plate digitally, the National Instrument NI DAQ system was used. The temperature module was model NI 9213 16-ch TC, 24-bit C series module, and chassis used was cDAQ-9172 8-slot USB 2.0 Chassis for CompactDAQ [26, 27]. The obtained values were processed through the National Instruments SignalExpress to be logged as Excel files into the computer. As discussed in subchapter 2.3.1, the temperature of the aluminum plate was measured with K-type thermocouples installed in the plate, measuring the temperature from the middle of the plate.

Although it was credible design, the aluminum plate design was regarded as unsuccessful for the intentions of this research, which is conducting experiments with discrete heat sources. Having a high thermal conductivity, the aluminum plate was expected to decrease the time needed to reach steady state. Additionally, having the 2.000 mm x 1.000 mm grooves machined onto the plate were expected to minimize the conduction effect from heater to heater. To validate the successful construction of the test section, the Nusselt number for forced convection over a flat plate with constant heat flux correlation and the local Nusselt number obtained from the experimental data were compared. The local Nusselt number for constant heat flux was taken from Ref. [28] is given as

$$Nu_x = 0.453 Re_x^{1/2} Pr^{1/3} \qquad \text{(Eq. 4.2)},$$

where x is the location, h is the convection heat transfer coefficient, Re_x is the local Reynolds number, Pr is the Prandtl number. Knowing the temperature of the plate, ambient temperature, thermal conductivity, and heat flux, the Nusselt number from the experiment can be also calculated.

The two Nusselt numbers matched at the lower fluid flow velocity (see Figure 4-1), but were then separated as the fluid velocity increased, as shown in and Figure 4-2. Figure 4-1 shows that the two Nusselt numbers match relatively well. In Figure 4-2, the difference between the Nusselt values is larger when the fluid velocity is increased, indicating that the measured temperature downstream of the plate is lower than expected value. Possibly, the separation of the two Nusselt numbers at higher velocity was due to the high thermal conductivity of the aluminum plate. As the flow velocity increased, the tip of the plate encountered a higher convection cooling rate, and the heat generated from downstream of the plate was conducted to the front, making it a conjugate heat transfer problem, rather than convection heat transfer problem with discrete heaters. This conjugated effect led to the second foam plate design, which used the foam as insulation between the discrete heating elements.

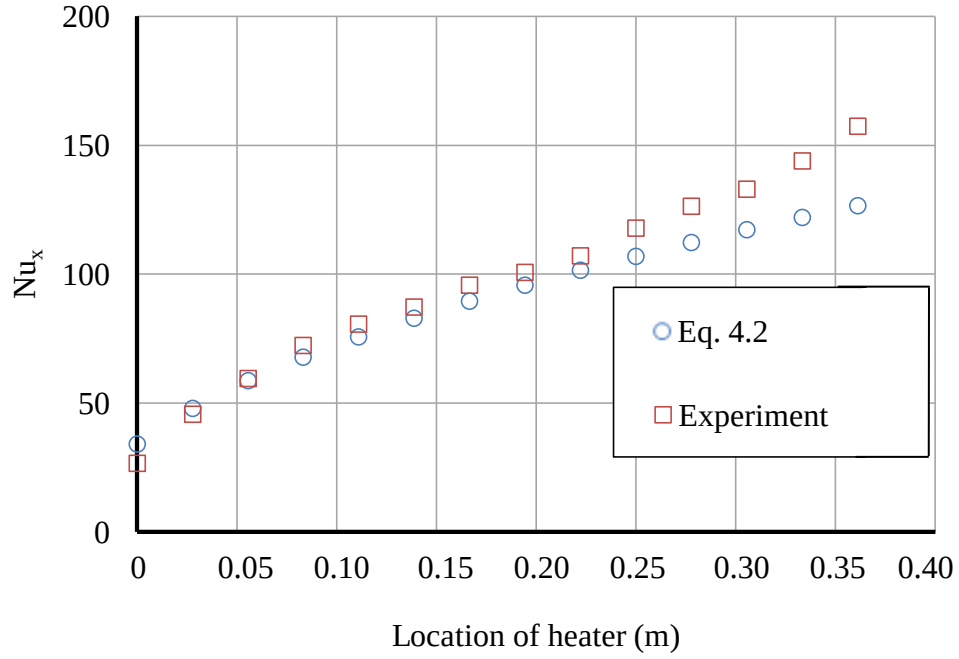

Figure 4-1 Constant Heat Flux, Nu_x vs. location, 3.7 m/s fluid velocity

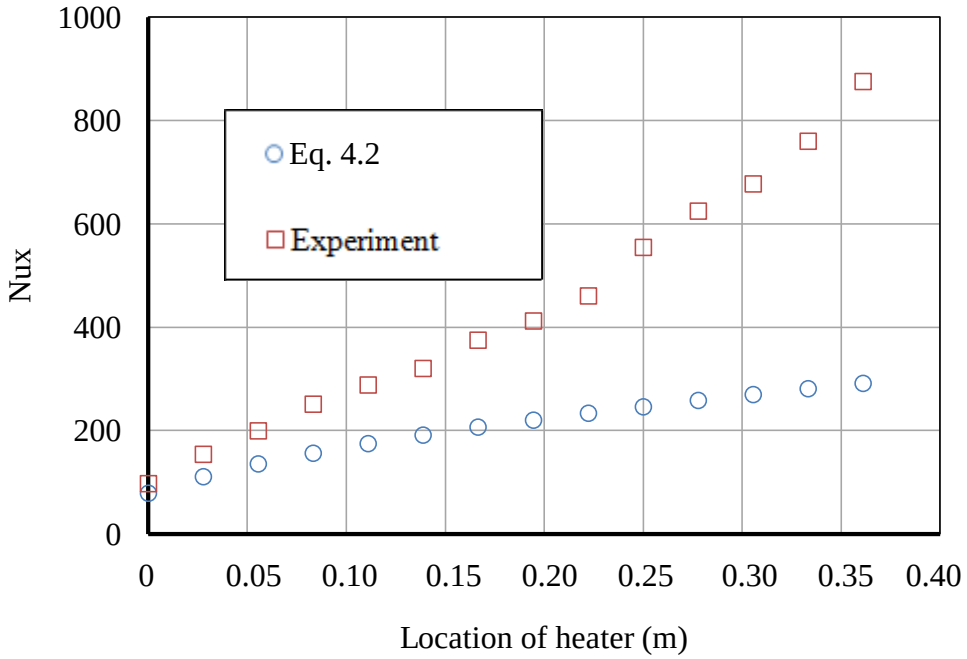

Figure 4-2 Constant Heat Flux, Nu_x vs. location, 17 m/s fluid velocity

4.2 Natural Convection Measurements

4.2.1 Thermocouple Assembly

The initial temperature measurement methodology for natural convection experiments with the foam plate used three thermocouples per heating element, which were installed under the aluminum plate, above the Kapton® heater. To confirm that the temperature measurement technique was valid without re-fabricating the existing plate with extra surface thermcouples, a replica of the foam plate assembly with a single heating element was constructed. The replica test sample had an additional K-type thermocouple attached to its aluminum surface.

From the test with the replica assembly, the measured average temperatures from underneath the plate was 4°C higher than the average temperatures measured with thermocouple on the outer surface of the plate. Using a one-dimensional conduction heat transfer equation from the equation 1.1 in the reference [28],

$$q_x'' = -k\frac{dT}{dx} \qquad \text{(Eq. 4.3)},$$

where k is the thermal conductivity, and dT/dx is the gradient of temperature in the x direction, the expected temperature difference was less than 0.001°C. Due to the imprecise temperature readings, caused by the smaller contact area of the thermocouple to the plate surface, the test results obtained with the first measurement technique were no longer valid.

To improve the surface temperature measurement technique, a E-type thermocouple with bare ribbon wire tips were installed on the top surface of one plate for the natural convection testing, the technique proposed in references [29, 30]. Using a

spot thermocouple welder, the tips of the 36 AWG E-type thermocouple wires were welded to thin ribbon wires. These ribbon type thermocouple wires were 0.050 inches wide and approximately 0.0005 inches thick. These ribbon wires were then also welded together to complete the thermocouple circuit. This assembly was then secured to the surface of the aluminum plate with a thin layer of 5-minute epoxy.

In addition to the new surface thermocouple measurement technique, the temperature was measured with an infrared (IR) camera [29]. For the results reported in Chapter 6, the temperature measurements were obtained with the IR camera, and the E-type surface thermocouple was used for the IR camera calibration purpose. The assembly and installation of E-type thermocouple are illustrated in Figure 4-3.

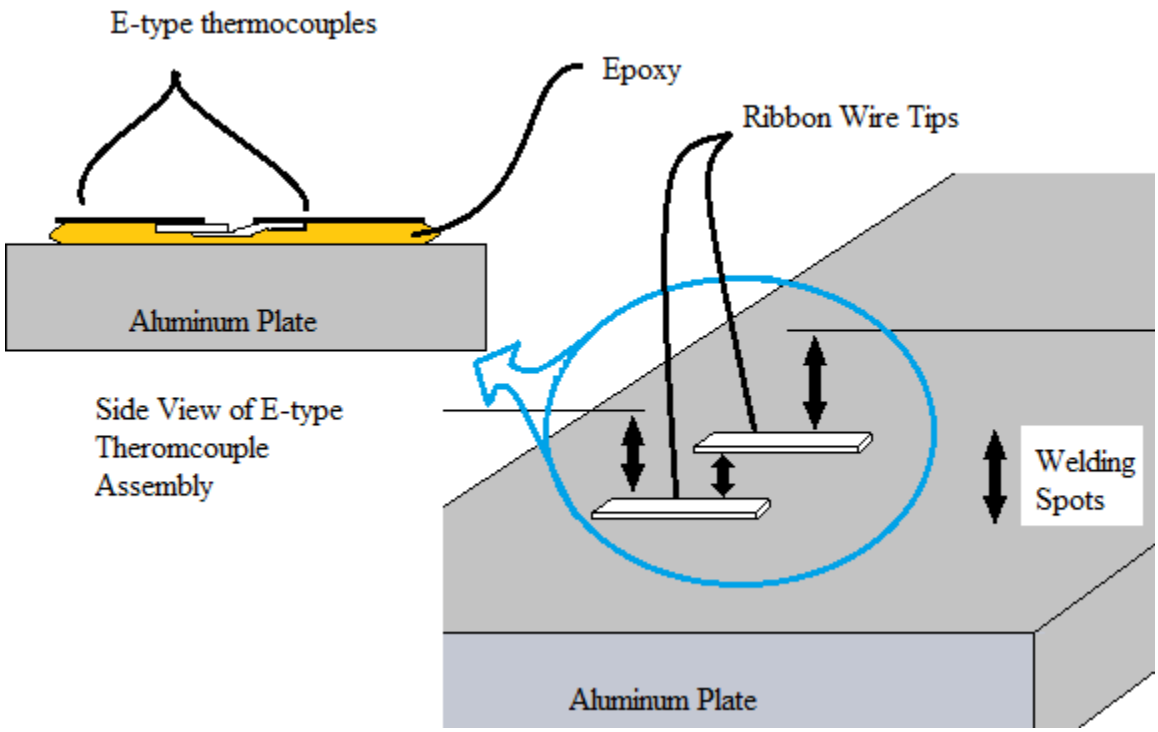

Figure 4-3 Surface thermocouple installation illustration

4.2.2 Calibration of Temperature Measurement

The calibration of the IR camera was a two-step process. The first step was calibrating the E-type thermocouples shown in Figure 4-3 to a thermistor. The second step was to calibrate the IR camera to the calibrated E-type thermocouple. The calibration of the E-type thermocouples was done using a constant temperature water bath, RTE 7 model chiller unit from Thermo Scientific and a high precision thermistor probe. Two E-type thermocouples were fabricated in the same way that was described in subchapter 4.2.1. Using the chiller, the two thermocouples and the thermistor probe were placed approximately 5 mm apart from each other, the thermistor probe being in the middle of the two thermocouples. To insulate the bare thermocouple tips from shorting in the water, the wires were coated with the same 5-minute epoxy that was used to coat and secure the thermocouple onto the test plate surface.

The calibration was done at several different temperatures, ranging from 30.00℃ to 69.00℃, since this was the expected temperature range for the natural convection tests. Even though the highest temperature difference between the probe and the two thermocouples was 0.411℃, and the root-mean-squared (RMS) value of that thermocouple tip was ±0.277℃, both measurements presented a much lower uncertainty value than the typical E-type thermocouple uncertainty, which is ±1.5℃. Although using the RMS value is the conventional way of estimating accuracy, the maximum temperature difference, ±0.411℃, was used for the uncertainty value of the installed thermocouple, which is a more conservative approach.

After calibrating the E-type thermocouple, this was installed onto the surface of the plate and the IR camera was calibrated. The temperature range for the second

calibration step was from 30.9℃ to 73.1℃. The maximum temperature reading difference between the IR camera and the installed E-type thermocouple was 0.395℃, and RMS value of ±0.182℃. The two temperature readings are graphed in Figure 4-4, which shows that the uncertainty value should be very small (i.e., the difference between the two measurement is minimal).

If the thermistor probe is assumed to measure the true reference temperature, then to calculate the uncertainty of the IR camera, one would have to add the uncertainties of the E-type thermocouple from the first step and the uncertainty of the IR camera from the second step. If the RMS values were taken to estimate the uncertainty of the IR camera, it would be ±0.331℃ (a conventional approach). However, the maximum difference values were taken to calculate the uncertainty of the IR camera in order to be conservative with the measured temperature data, and the uncertainty becomes ±0.570℃. The collected data for the calibration tests are given in Appendix C.

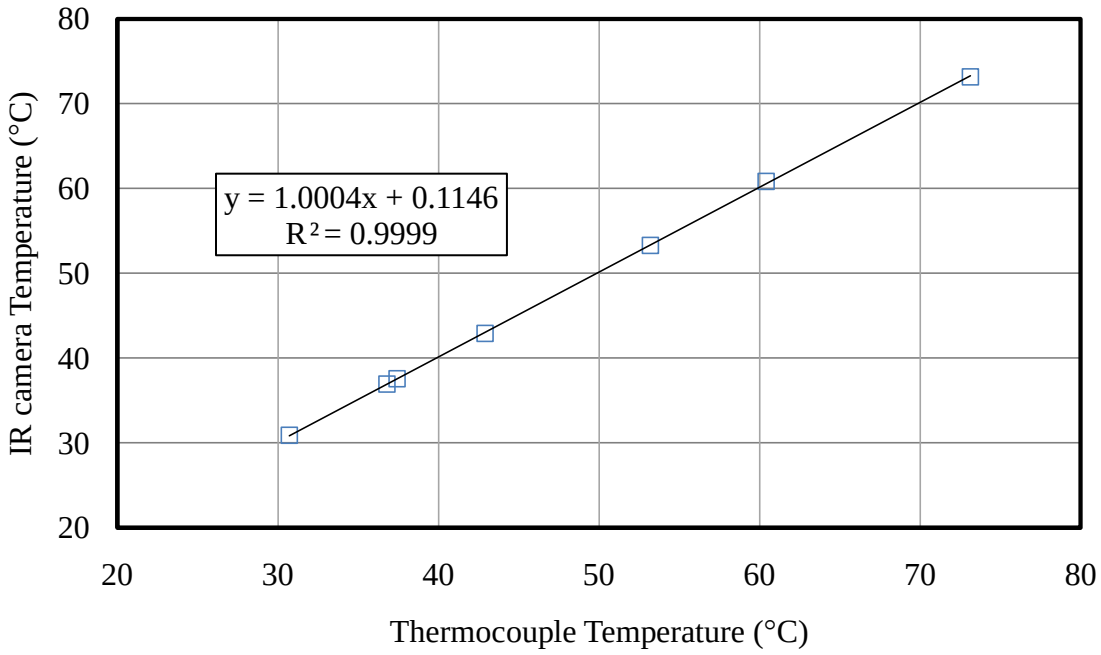

Figure 4-4 Infrared camera calibration graph

From these results, it can be shown that the IR camera has a very low uncertainty value, less than ±1℃, and will provide good measurements of the surface temperature, without the need of installing surface thermocouples onto every heater on the plate. Note that one thermocouple was installed on one plate for calibration purposes only.

Chapter 5 Experimental Procedure - Natural Convection

5.1 Supplying Power

For the natural convection tests, only the first three heaters of the five designed heaters were used. The power was supplied to the heaters using a variable autotransformer, as known as VARIAC, and a DC power supply PSU304 (DC power supply) from Omega Engineering, Inc. Due to limitations of the maximum voltage output from the DC power supply, the VARIAC was used when the voltage supplied to the heaters exceeded the maximum voltage output of the DC power supply. The DC power supply displayed the voltage and current values during the experiments, while the VARIAC only controls the voltage output. Therefore, the VARIAC required the usage of Agilent U3401A multimeter to measure the supplied voltage. This multimeter has an exceptional DC voltage reading accuracy, ±0.02% basic accuracy, so the power supplied by the VARIAC can be considered highly accurate [31].

While using the DC power supply, the controlled voltage was supplied to one heating element at a time, and the current being supplied to the circuit was monitored. Plotting the displayed current versus supplied power gave a correlation between the two variables as (Figure 5-1):

$$I=0.0118V+.0013 \qquad \text{(Eq. 5.1).}$$

Also, to calculate the resistance of the circuit and the power dissipation, the two equations below were used in conjunction with the obtained data.

$$V=IR \qquad \text{(Eq. 5.2)}$$

$$P=VI \qquad \text{(Eq. 5.3)}$$

where P is power, V is voltage and R is resistance.

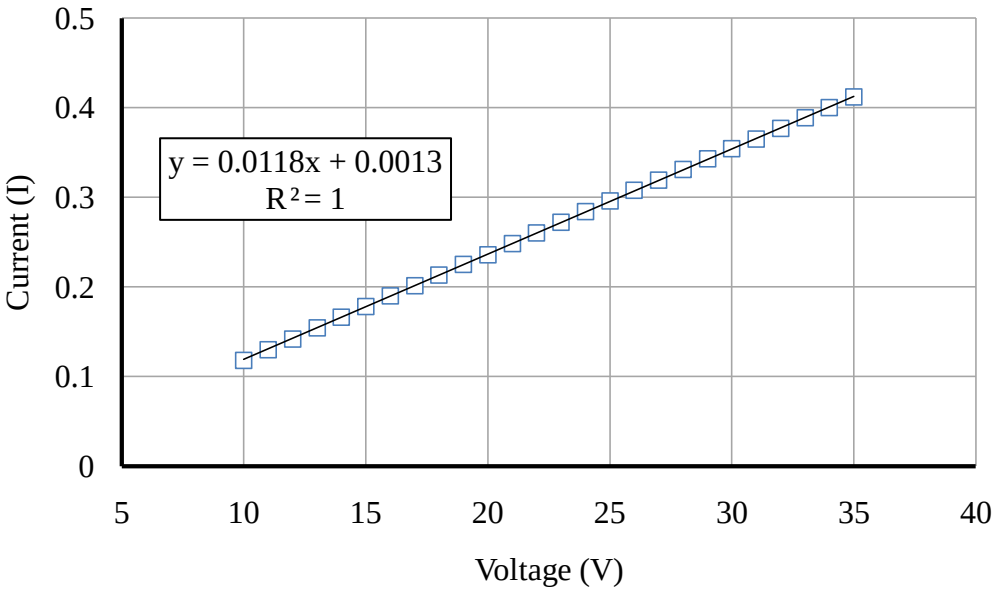

Figure 5-1 Averaged current vs. voltage, for all 5 heating elements

The nominal resistance value at the supplied voltage, which ranges from 10V to 35V, was 84.605 ohms with an uncertainty of ±0.2029 ohms, which translates to ±0.2% accuracy of the measured resistance. This returns the lower accuracy than the DC power supply voltage accuracy (±0.02% of the readings), but still a very highly accurate [32]. Note that the resistances of the heaters do not change for the supplied voltage range, so the relation between the voltage and the current can be assumed linear. Finally, by combining (Eq. 5.1) and (Eq. 5.3),

$$P=V(0.0118V+0.0013) \quad \text{(Eq. 5.4)}$$

was obtained. This equation is important because the multimeter, which was connected to the VARIAC during experiments, can only display either voltage or current at a time,

and Eq. 5.4 enables the calculation of power from knowing only the voltage. Since the Eq. 5.4 is only function of voltage and the voltage accuracy of the DC power supply is ±0.2% of the readings, one can estimate that the accuracy of the supplied power would only be ±0.45% of the calculated power from Eq. 5.4.

5.2 Test Matrix and Measurement Process

The first set of tests was conducted dissipating an equal amount of heat throughout the all three heaters i.e., uniform heat flux. The second set of tests consisted of distributing an equal wattage to two heaters while varying the location. For example, with a total power dissipation of 22.24 [W], the first and the second, the first and the third, then the second and the third heaters were heated with equal power dissipation rates (i.e., 11.12 [W] each). The third testing condition varied the power dissipation ratios between two heaters. For this set of tests, the second heater was not heated. The power output ratios between the two heaters (i.e., q_1''/q_3'') were varied from 2:1 to 1:5. These power output ratios were tabulated by distributing the total output to different number of heaters, and the ratio of the distributed power is given as the "Ratio" column in Table 5-1. If the "Ratio" is 0, it indicates that the heater is not being heated. For example, for Test #3, the third column under Ratio category, the first heater dissipates 13.344 [W], the second heater 0 [W], and the third heater 8.869 [W], adding up to total of 22.24 [W]. The exact details on how the test conditions were set is given in Table 5-1 and the heater numbers are given in Figure 5-2.

Table 5-1 Test condition matrix

Test #	Total Power [W]	Heater #	Power Dissipation Ratio															
1	24.15	1	1				1.1				1.25				1.5			
		2	0				0				0				0			
		3	1				1				1				1			
2	22.24	1	1	1	0	0	1	1	2	2	0	1	1	0	1	3	4	5
		2	1	0	1	0	0	1	1	0	2	2	0	1	0	0	0	0
		3	1	0	0	1	1	0	0	1	1	0	2	2	3	1	1	1
3	22.24	1	1.1				1.25				1.5							
		2	0				0				0							
		3	1				1				1							
4	15.96	1	1			1.05			1.1			1.25			1.5			
		2	0			0			0			0			0			
		3	1			1			1			1			1			
5	13.45	1	1			1			0			0						
		2	1			0			1			0						
		3	1			0			0			1						
6	9.45	1	1			1.05			1.1			1.25			1.5			
		2	0			0			0			0			0			
		3	1			1			1			1			1			

While supplying the power to the heaters, the ambient temperature was recorded using the NI-DAQ. From the collected data, it was shown that the ambient temperature was controlled very well between 23℃ to 24℃. This was recorded using the NI SignalExpress and the average temperature value recorded during each test was used as the ambient temperature, T_{∞}.

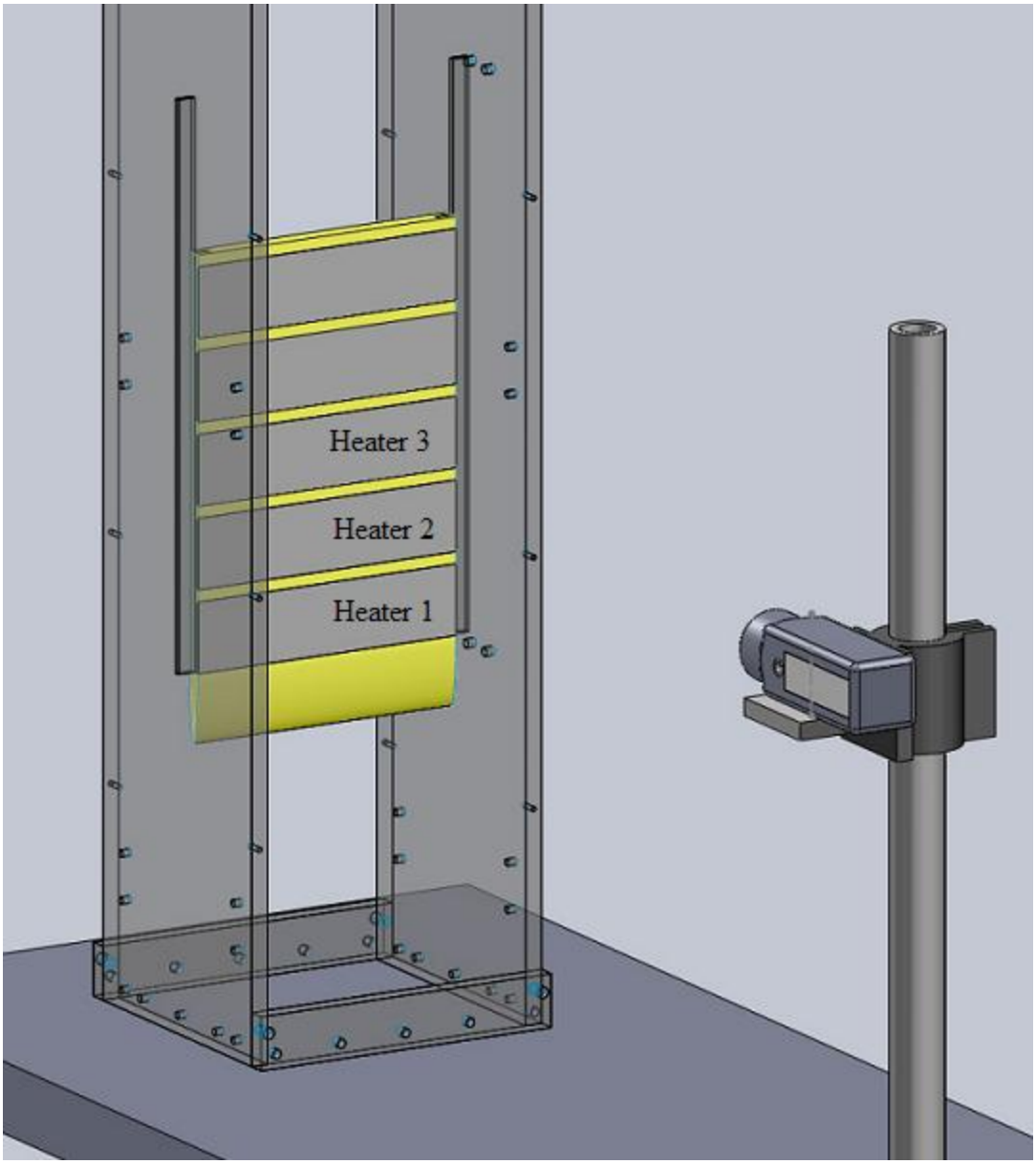

Figure 5-2 Enlarged view of natural convection test setup. Heater numbers denoted.

The surface temperature of the plate was measured using the IR camera as mentioned in subchapter 4.2.2. Using the "Profile" function of the installed IR camera program, a temperature profile of a drawn line in the camera image was visualized. The

steady state of the plate was monitored by selecting a point in the obtained image and observing a "temporal plot". The "temporal plot" function showed the temperature change of the selected pixel over time. When the temperature change of the "temporal plot" becomes less than 0.5℃ difference within the 10 minute period, the IR camera image was then collected three times. Each data collection was set 5 minutes apart.

5.3 Test Section Validation

To validate the natural convection measurements, the Nusselt number for natural convection with constant heat flux conditions on a vertical plate from an established correlation and the calculated Nusselt number from the experiments data were compared. The Nusselt number correlation for constant heat flux natural convection is given in the Ref. [33]:

$$Nu_y = 0.644 Pr^{1/5} Ra_{*y}^{1/5} \qquad \text{(Eq. 5.5)}$$

where Ra_{*y} is Rayleigh number, $Ra_{*y}=g\beta y^4 q''/\alpha\nu k$, based on the height of the foam plate, Pr is the Prandtl number, g is the gravity, β is thermal expansion coefficient, y is height of the plate at the point of interest, α is thermal diffusivity, and ν is kinematic viscosity of the air at the given temperature. All properties except g and y are temperature dependent and were calculated using the measured ambient temperature. The calculation to obtain properties of ambient air was done by interpolating the given data in reference [33] at the measured ambient temperature.

The local Nusselt number from the experimental data was computed using the equation 4.72 in the reference [33],

$$Nu_y = \frac{q''}{(T_o(y)-T_\infty)} \frac{y}{k} \qquad \text{(Eq. 5.6)}$$

where $T_o(y)$ is the local surface temperature at location y. The Figure 5-3 shows the temperature difference between the local temperature of the foam plate and the ambient temperature in the y-axis.

The difference was graphed against the location where the temperature was measured along the plate (x-axis). The figure shows that in the unheated or insulated region from 0.05m to 0.06m, and 0.11m to 0.12m, the temperature was still considerably high, approximately 25℃ higher than the ambient temperature. So when calculating the heat flux of the plate, the area of the interest became larger than just the area of aluminum plates—the power dissipating surface area was enlarged to include the small insulation region between the heaters. This was because the foam spacers were also heated to temperatures significantly higher than the ambient temperature value, indicating these areas were also dissipating heat to the surroundings.

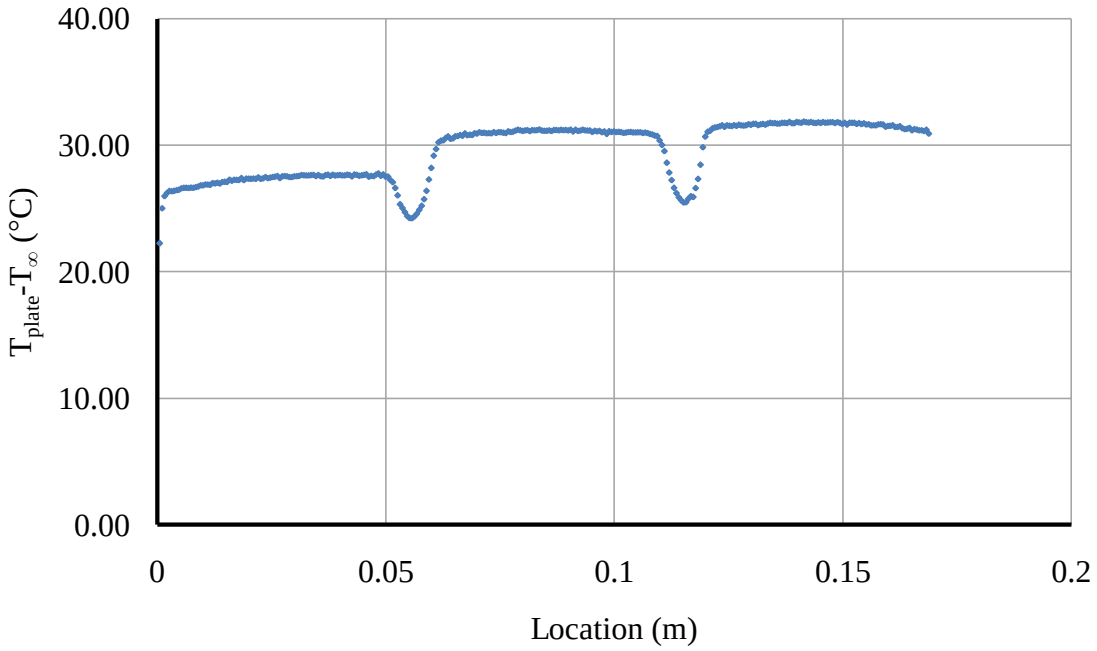

Figure 5-3 T_{plate}-T_∞ vs. Location along the plate, 22.24 [W] distributed evenly

With a power dissipation of the 22.24 [W], the two Nusselt numbers agree well, which is an indication that the plate assembly works as it was predicted is shown in Figure 5-4. The two locations where the experimental Nusselt number spikes are due to the low temperature region of the foam spacers. As can be seen, the two Nusselt values deviate downstream of the plate, which maybe an indication that the flow reaches near transition region, as confirmed by the Rayleigh number, of 6.19E+08.

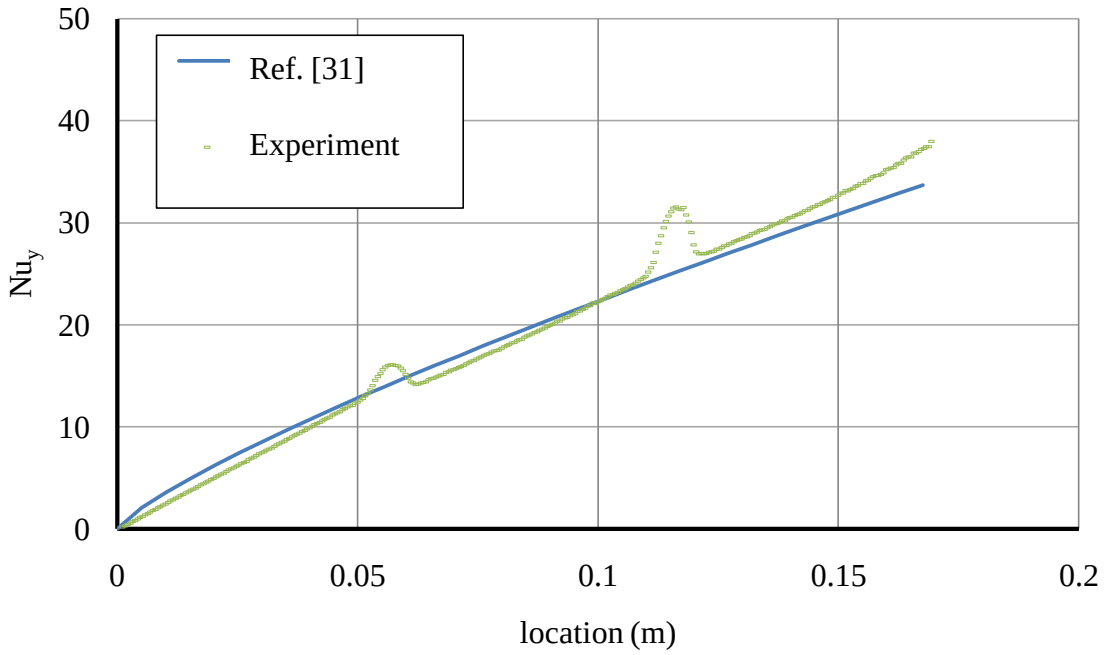

Figure 5-4 Nu_y vs. Location, at 22.24 [W], distributed evenly through all three heaters. Validation test

Chapter 6 Results

In this section, the obtained data was used to find the combinations of geometrical location of heaters and power dissipation ratios between the heaters that would result in the maximized thermal conductance,

$$C = \frac{Q'}{k(T_{max}-T_{\infty})} \qquad \text{(Eq. 6.1)}$$

where C is the thermal conductance, Q′ is the total heat current through the heating elements [12]. The maximum thermal conductance value would be achieved when the difference between the test plate and ambient temperatures is at minimum, i.e., the minimized maximum temperature [12].

To illustrate the effect of geometrical placement of heaters with equal heat dissipation rate, a set of tests was conducted while supplying a total of 22.24 [W] to the entire plate. For instance, in Chapter 5, Figure 5-3 shows the equal distribution of power dissipation rate over the three heaters, and the maximum value of $T_{plate,max}$-T_{∞} (ΔT), measured at the third heater, of (31.22℃); $T_{plate,max}$ denotes the maximum temperature of the test plate. If the total power dissipation rate was distributed to two consecutive heaters equally, the maximum temperature difference was measured at the most downstream heater, ΔT reaching up to 40.15℃. When the first and the third heaters were dissipating 11.12 [W] each, ΔT was measured at 36.21℃, as shown in Figure 6-2. When a single heater is dissipating the total heat, the ΔT of the plate reaches above 60℃, shown in Figure 6-1. Figure 6-2 shows the temperature profile of the plate when two heaters are dissipating same amount of heat, while varying the location of the heaters.

When all of the geometrical placements and the number of heaters were considered (i.e., comparing Figures 5-2, 6-1, and 6-2), it was observed that it would be the most practical to dissipate the heat throughout the entire surface of the plate. However, if only two or less heating elements can be considered, it is the combination of the first and the third heater that results in the lowest maximal temperature of the plate.

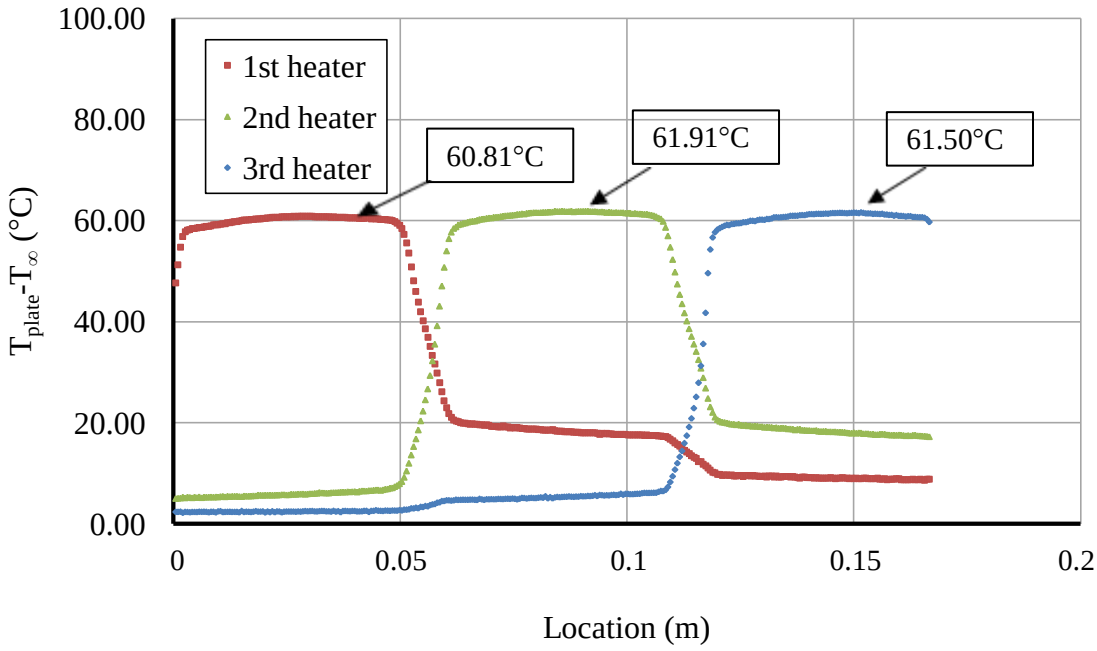

Figure 6-1 ΔT vs. the location of the heaters. Single heater dissipating 22.24 [W]. Variation in geometry.

Now that the optimal locations of the discrete heat sources were found with the given constraints, the power dissipation ratio between the heaters can be optimized. With the first and third discrete heating elements connected to the power supply, the dissipation ratios between the two heaters were varied at different wattages. By plotting the data obtained from Test # 2 in Table 5-1, the maximum temperature of the plate was

the lowest when the power dissipation ratio was 1 to 1 (Figure 6-3), with the given test conditions. Based on this result, the optimal distribution of power dissipation should lie near 1 to 1 ratio.

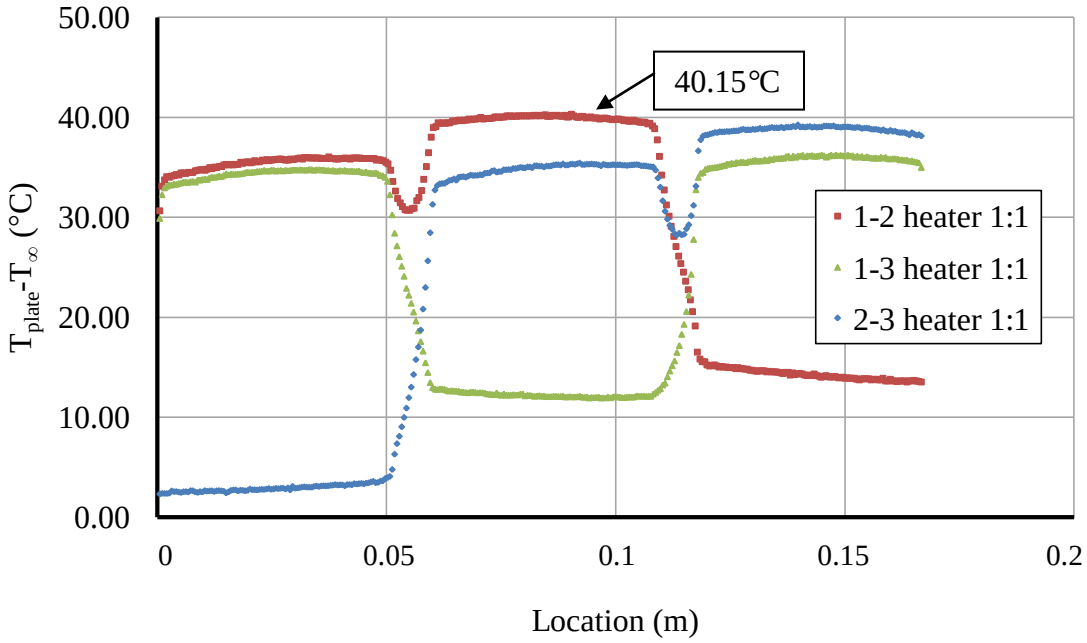

Figure 6-2 T_{plate}-T_∞ vs. the location of the heaters. Two heaters are dissipating the equal amount of heat. Varied geometry. Total wattage output is 22.24 [W]

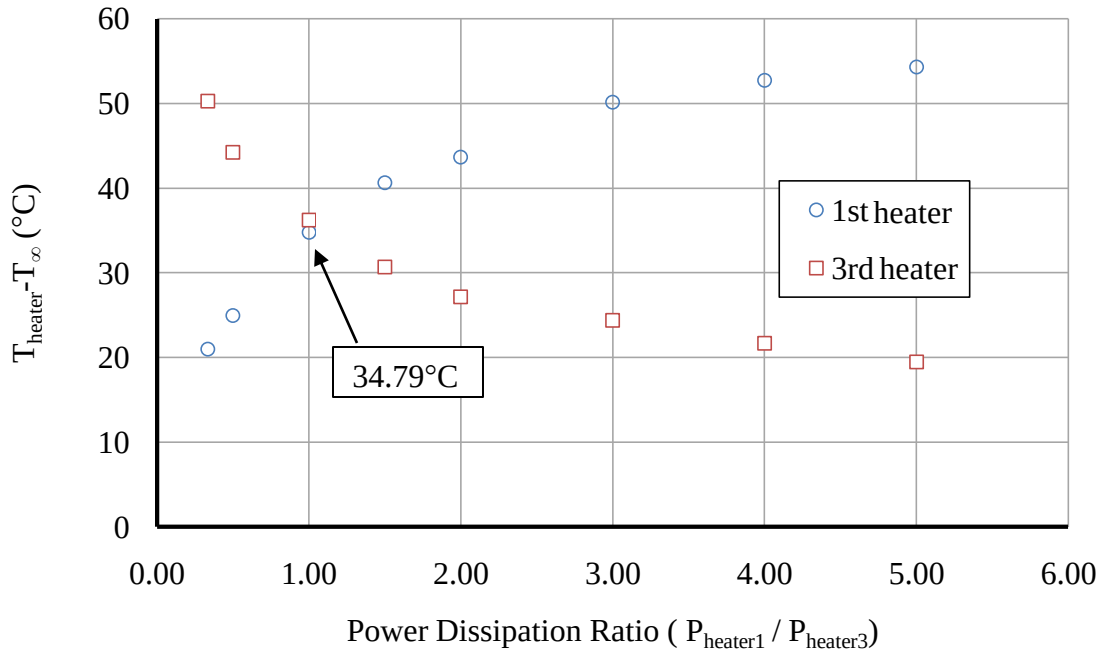

Figure 6-3 ΔT vs. Power Ratio. Total power output of 22.24 [W]. The minimum value of maximum temperature lies near 1 to 1 ratio

As the initial 22.24 [W] experiments revealed that the optimal power dissipation ratio for the given test conditions were close to 1, subsequent experiments focused on varying the dissipation ratios in smaller increment to find the more accurate dissipation ratio between the heated elements. The experimental results from smaller increment tests (i.e., Test #1, #4, and #5) are given in Table 6-1. For the range of wattage tested, the minimized maximum temperature was achieved when the power dissipation from the first heater ($P_{heater1}$) to that of the third heater ($P_{heater3}$) is between 1.05 and 1, resulting in the maximized thermal conductance value should be located.

Table 6-1 Results from Test #1, #4 and #6. Smallest absolute difference of maximum temperature values of each heater is approximately at 1.05 to 1 ratio

Test #1 (24.15 [W])	$P_{heater1}/P_{heater3}$	1/1	1.1/1	1.25/1	1.5/1	
	ΔT_{1max} (°C)	37.22374	38.22461	41.24776	42.91048536	
	ΔT_{3max} (°C)	38.63508	37.10282	36.11831	33.41176536	
	ΔT_{1max}-ΔT_{3max}	-1.41134	1.12179	5.12945	9.49872	
	V1 (volts)	32	32.706	33.731	35.08	
	V3 (volts)	32	31.19	30.165	28.61	
Test #4 (15.96 [W])	$P_{heater1}/P_{heater3}$	1/1	1.05/1	1.1/1	1.25/1	1.5/1
	ΔT_{1max} (°C)	27.4326	27.64806	28.11088	29.025452	30.6104
	ΔT_{3max} (°C)	28.27602	27.47384	26.75823	25.260482	23.35983
	ΔT_{1max}-ΔT_{3max}	-0.84342	0.17422	1.35265	3.76497	7.25057
	V1 (volts)	26	26.316	26.613	27.408	28.485
	V3 (volts)	26	25.68	25.372	24.51	23.25
Test #6 (9.45 [W])	$P_{heater1}/P_{heater3}$	1/1	1.05/1	1.1/1	1.25/1	1.5/1
	ΔT_{1max} (°C)	17.30054	17.39881	17.95703	18.766454	19.89895
	ΔT_{3max} (°C)	17.95488	17.43937	17.16504	16.379164	15.3423
	ΔT_{1max}-ΔT_{3max}	-0.65434	-0.04056	0.79199	2.38729	4.55665
	V1 (volts)	20	20.242	20.472	18.853	21.915
	V3 (volts)	20	19.752	19.517	21.09	17.866

It was also found that increasing the total power dissipation increases the temperature difference between the ΔT of each heating element, even at the same power dissipation ratio. Figure 6-4 shows how the difference between each heater increases as the total wattage increases. Notice that this is true for all heat dissipation ratios studied. This means that as the total wattage supplied to the entire plate gets higher, the exact power dissipation ratios between the heaters that would minimize the ΔT value becomes easier to find. The obtained result can also be shown by comparing the thermal conductance values of each test conditions (Figure 6-5). This figure shows that the

maximum thermal conductance lies near 1.05 to 1 power dissipation ratio between the first and the third heaters, at a given total wattage.

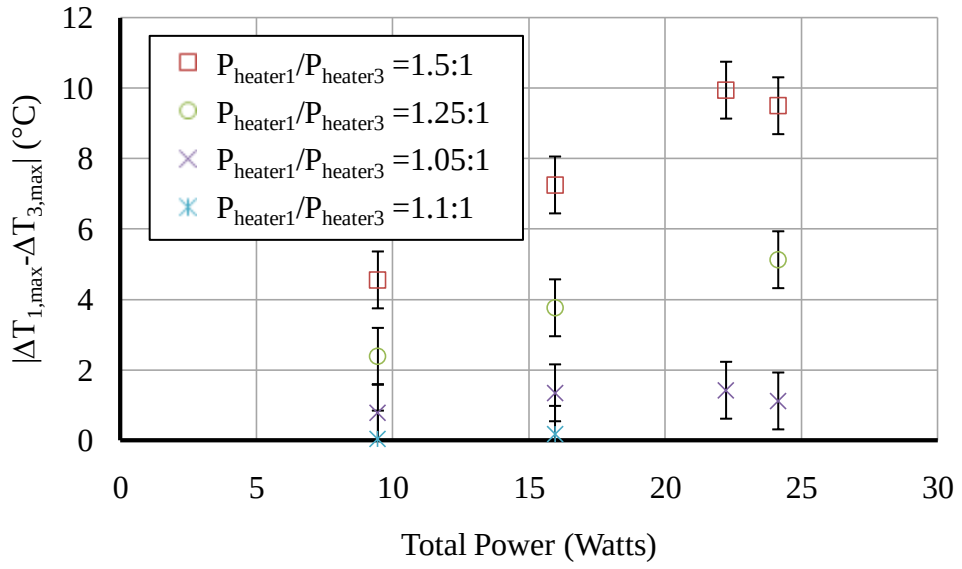

Figure 6-4 The absolute difference between the ΔT_{1max} and ΔT_{3max}

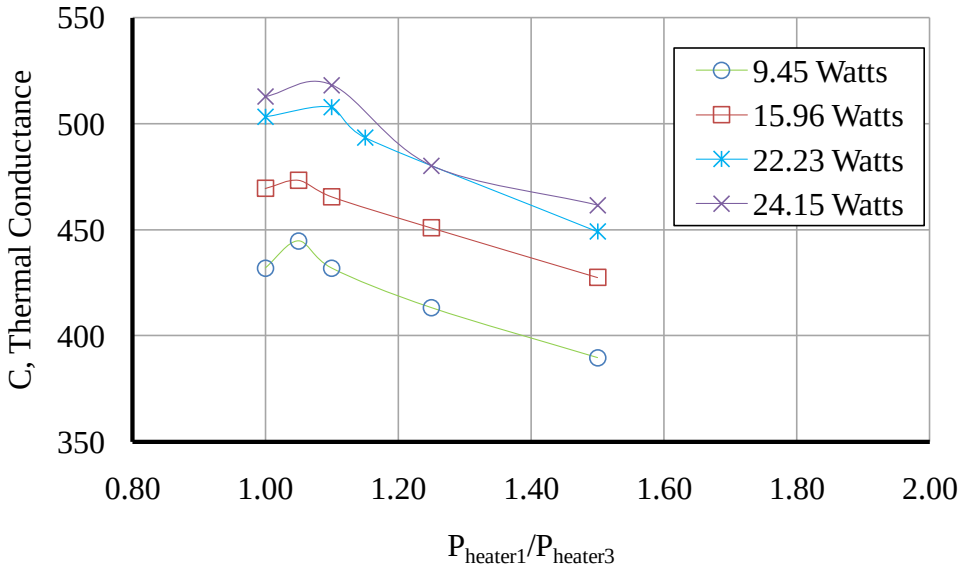

Figure 6-5 Thermal conductance vs. Power dissipation ratio at different wattages

Chapter 7 Conclusion and Suggested Future Work

7.1 Overall Summary

The objective of this research was to fabricate an experimental setup to test the cooling of discrete heating elements. There were two plate designs; aluminum plate design for forced convection experiments and R3315 foam design for natural convection experiments.

Due to the high thermal conductivity of the aluminum plate, the design was regarded as unsuitable for the purpose of testing the discrete heating elements. The foam plate design isolated discrete heaters appropriately and natural convection tests were conducted using the second design. Along with the new plate design, an IR surface temperature measurement technique [29, 30], enabled the temperature measurements to be highly accurate.

For the natural convection experiments, a test matrix was created to find the optimal geometrical location of the discrete heaters and their power dissipation ratios with given constraints that would maximize the thermal conductance. The thermal conductance was the highest when the first and third heaters are dissipating heat with the dissipation ratios from 1.05 to 1.

7.2 Suggested Work

The suggested work for the future is conducting more tests with increased total power dissipation rate to find more accurate optimal power dissipation ratio between the first and the third plates. The geometry also can be varied, using all the five heaters installed on the plate. Furthermore, if the forced convection experiments were to be conducted using the revised temperature measurement method, then an IR window, such

as Zinc Selenide or Sodium Chloride window, should be installed onto the walls of the wind tunnel. The IR camera then needs to be recalibrated to insure the correct temperature measurement through the IR window. The forced convection experiments should also be aimed at finding the maximum thermal conductance with some specified constraints.

Appendix A

Nomenclature

C – Thermal Conductance

Nu_x – Local Nusselt Number, in x-axis

Nu_y – Local Nusselt Number, in y-axis

Q' – Total heat current through the heating elements (W/m)

k – Thermal conductivity (W/mK)

T_{max} – Maximum temperature (℃)

T_{plate} – Plate temperature (℃)

T_{heater} – Discrete heating element temperature (℃)

ΔT – Temperature difference between the plate and the ambient (℃)

$P_{dynamic}$ – Dynamic pressure (N/m^2)

ρ – Density of air (kg/m^3)

v– Velocity of fluid (m/s)

ν – Kinematic viscosity (kg/m^3)

q_x'' – Heat flux (W/m^2)

V – Voltage(V)

I – Current (Amps)

P – Power (W)

R – Resistance (Ohms)

Ra_{*y} – Rayleigh number based on the height

β – Thermal expansion coefficient (1/K)

α – Thermal diffusivity (m^2/s)

g – Gravity

T_∞ - Ambient temperature (K)

Appendix B

Properties of R3315 Foam

LAST-A-FOAM® R-3315 RIGID POLYURETHANE FOAM			
Property	English	Metric	Test Method
Density (pcf) (kg/m^3)	15.0	240	ASTM D-1622
Compressive Strength (psi) (kPa)			ASTM-D-1621
Parallel to Rise			
@ 75℉	679	4682	
@ 200℉	398	2747	
Perpendicular to Rise			
@ 75℉	696	4798	
@ 200℉	430	2962	
Compressive Modulus (psi) (kPa)			ASTM-D-1621
Parallel to Rise			
@ 75℉	16165	111458	
@ 200℉	11700	80672	
Perpendicular to Rise			
@ 75℉	16779	115691	
@ 200℉	10958	75555	
Tensile Strength (psi) (kPa)			ASTM D-1623 Type A Specimens
Parallel to Rise	646	4454	
Perpendicular to Rise	684	4717	
Tensile Modulus (psi) (kPa)			ASTM D-1623 Type A specimens
Parallel to Rise	31456	216890	
Perpendicular to Rise	26068	179735	
Shear Strength (psi) (kPa)			ASTM C-273 Compression Shear
Rise Parallel to Specimen Length	506	3489	
Rise Parallel to Specimen Thick.	533	3674	
Shear Modulus (psi) (kPa)			ASTM C-273 Compression Shear
Rise Parallel to Specimen Length	4701	32413	
Rise Parallel to Specimen Thick.	5012	34558	
Flexural Strength (psi) (kPa)			ASTM D-790 Method 1-A
Rise Parallel to Specimen Width	1057	7289	
Rise Parallel to Beam Thick.	1048	7227	
Flexural Modulus (psi) (kPa)			ASTM D-790 Method 1-A
Rise Parallel to Specimen Width	27927	192557	
Rise Parallel to Beam Thick.	27084	186744	
CTE: (in/in/℉) (K^-1)	~3.4 x 10^-5	~6.1 x 10^-5	From -40 to +200℉, GP Method
Thermal Conductivity "k":			ASTM C-518 at 75℉ (24℃) mean temp.
(BTU*in/ft^2*℉*h) [(W/m*K)]	0.307	0.044	
Hardness, Shore-D (cut foam surface)	27.0	27.0	ASTM D-2240
Tumbling Friability - weight loss (%)	2.8	2.8	ASTM C-421 (20 minutes @ 60 rpm)

Source: http://www.generalplastics.com/uploads/pdf/R-3315Eng-Metric.pdf?PHPSESSID=2811048beb84aaf751abfe581909e24b

Appendix C

Uncertainty Data

Table 0-1 IR camera vs. Thermocouple Calibration Data

IR (℃)	E-type Thermocouple (℃)	IR-E-type (℃)
37.54	37.43	0.11
60.819	60.424	0.395
42.9	42.913	-0.013
30.904	30.702	0.202
53.248	53.2003	0.0477
73.172	73.1184	0.0536
36.932	36.793	0.139

Table 0-2 Thermocouple vs. Thermistor Calibration Data

Set T (℃)	E-type (℃)		Thermistor (℃)	T1-Thermistor (℃)	T2-Thermistor (℃)
	1	2			
69	69.5333	69.2917	69.209	0.3243	0.0827
	69.5428	69.301	69.208	0.3348	0.093
	69.5307	69.2995	69.203	0.3277	0.0965
68.5	69.0887	68.8588	68.697	0.3917	0.1618
	69.1043	68.8589	68.698	0.4063	0.1609
	69.0993	68.8345	68.698	0.4013	0.1365
60	60.5383	60.2957	60.138	0.4003	0.1577
	60.5222	60.2895	60.137	0.3852	0.1525
	60.5413	60.3119	60.137	0.4043	0.1749
59	59.5496	59.3262	59.166	0.3836	0.1602
	59.5301	59.292	59.141	0.3891	0.151
	59.5232	59.2968	59.143	0.3802	0.1538
50	50.5818	50.3685	50.21	0.3718	0.1585
	50.6291	50.4317	50.295	0.3341	0.1367
	50.7241	50.4971	50.543	0.1811	-0.0459
45	45.4553	45.2457	45.14	0.3153	0.1057
	45.4828	45.2617	45.101	0.3818	0.1607
	45.4665	45.2673	45.055	0.4115	0.2123
40	40.4504	40.2372	40.063	0.3874	0.1742
	40.4321	40.2305	40.06	0.3721	0.1705
	40.4361	40.1896	40.061	0.3751	0.1286
35	35.2992	35.147	35.003	0.2962	0.144
	35.3164	35.1497	35.053	0.2634	0.0967
	35.3248	35.1527	35.06	0.2648	0.0927
30	30.4025	30.2634	30.065	0.3375	0.1984
	30.4641	30.2668	30.061	0.4031	0.2058
	30.4692	30.2644	30.06	0.4092	0.2044
Maximum				0.4115	0.2123

Glossary

Through Extrusion – A component of material formed by the process of extruding through a material

Extrusion Cut – A feature of a material that is hollowed by given depth

Thermal conductivity – Material's ability to conduct heat

AWG – American Wire Gauge. A standardized wire gauge used predominantly in the U.S.A.

Nusselt Number – Ratio of convective to conductive heat transfer rate across a boundary

Bibliography

1. Association, C.E. *CEA Announces Latest HDTV Sales Numbers*. 2004 [cited 2011; Available from: http://www.ce.org/Press/CurrentNews/press_release_detail.asp?id=10558.
2. Trends, D. *2011 Smartphone market share, by country*. 2011 [cited 2011; Available from: http://www.onlinemarketing-trends.com/2011/04/smartphone-marketshare-2011-italyus-aus.html.
3. Roberts, J., et al., *Stresses IN Area Array Assemblies Subjected to Thermal Cycling*. Imce2009: Proceedings of the Asme International Mechanical Engineering Congress and Exposition, Vol 5, New York: Amer Soc Mechanical Engineers. 267-278.
4. Shaw, H.J. and W.L. Chen, *Laminar Forced-convection in a Channel with Arrays of Thermal Sources.* Warme Und Stoffubertragung-Thermo and Fluid Dynamics, 1991. **26**(4): p. 195-201.
5. da Silva, A.K., S. Lorente, and A. Bejan, *Optimal distribution of discrete heat sources on a plate with laminar forced convection.* International Journal of Heat and Mass Transfer, 2004. **47**(10-11): p. 2139-2148.
6. da Silva, A.K. and L. Gosselin, *Evolutionary placement of discrete heaters in forced convection.* Numerical Heat Transfer Part a-Applications, 2008. **54**(1): p. 20-33.
7. Aminossadati, S.M. and B. Ghasemi, *A numerical study of mixed convection in a horizontal channel with a discrete heat source in an open cavity.* European Journal of Mechanics B-Fluids, 2009. **28**(4): p. 590-598.
8. Guimaraes, P.M. and G.J. Menon, *Combined free and forced convection in an inclined channel with discrete heat sources.* International Communications in Heat and Mass Transfer, 2008. **35**(10): p. 1267-1274.
9. Cui, C., X.Y. Huang, and C.Y. Liu, *Forced convection in a porous channel with discrete heat sources.* Journal of Heat Transfer-Transactions of the Asme, 2001. **123**(2): p. 404-407.
10. da Silva, A.K., S. Lorente, and A. Bejan, *Optimal distribution of discrete heat sources on a wall with natural convection.* International Journal of Heat and Mass Transfer, 2004. **47**(2): p. 203-214.
11. Dias, T. and L.F. Milanez, *Natural convection due to a heat source on a vertical plate.* International Journal of Heat and Mass Transfer, 2004. **47**(6-7): p. 1227-1232.
12. da Silva, A.K., G. Lorenzini, and A. Bejan, *Distribution of heat sources in vertical open channels with natural convection.* International Journal of Heat and Mass Transfer, 2005. **48**(8): p. 1462-1469.
13. Heindel, T.J., F.P. Incropera, and S. Ramadhyani, *Laminar natural convection in a discretely heated cavity .2. Comparisons of experimental and theoretical results.* Journal of Heat Transfer-Transactions of the Asme, 1995. **117**(4): p. 910-917.
14. Muftuoglu, A. and E. Bilgen, *Natural convection in an open square cavity with discrete heaters at their optimized positions.* International Journal of Thermal Sciences, 2008. **47**(4): p. 369-377.

15. Wang, G.X., H.L. Zhang, and W.Q. Tao, *Numerical-simulation of Natural-convection in Rectangular Enclosures with Discrete Heated Elements*, in *Heat Transfer in Electronic and Microelectronic Equipment*, A.E. Bergles, Editor. 1990. p. 197-209.
16. Ghasemi, B. and S.M. Aminossadati, *Numerical simulation of mixed convection in a rectangular enclosure with different numbers and arrangements of discrete heat sources.* Arabian Journal for Science and Engineering, 2008. **33**(1B): p. 189-207.
17. Ermolaev, I.A. and A.I. Zhbanov, *Mixed Convection in a Vertical Channel with Discrete Heat Sources at the Wall.* Fluid Dynamics, 2009. **44**(4): p. 511-516.
18. Tso, C.P., G.P. Xu, and K.W. Tou, *An experimental study an forced convection heat transfer from flush-mounted discrete heat sources.* Journal of Heat Transfer-Transactions of the Asme, 1999. **121**(2): p. 326-332.
19. Ebert, A., C. Resagk, and A. Thess, *Experimental study of temperature distribution and local heat flux for turbulent Rayleigh-Benard convection of air in a long rectangular enclosure.* International Journal of Heat and Mass Transfer, 2008. **51**(17-18): p. 4238-4248.
20. Tao, H.Z., et al., *Experimental study of heat transfer performance in a flattened AGHP*. Applied Thermal Engineering, 2008. **28**(14-15): p. 1699-1710.
21. Omega Engineering, I. *Resistance Heating Ribbon Wire*. 2008 [cited 2008; Available from: http://www.omega.com/pptst/NCRR_Series.html.
22. Company, G.P.M. *LAST-A-FOAM® R-3300*. 2011 [cited 2011; Available from: http://www.generalplastics.com/products/product_detail.php?pid=16&.
23. Omega Engineering, I. *Kapton® (Polyimide Film) Insulated Flexible Heaters*. 2009 [cited 2009; Available from: http://www.omega.com/pptst/KHR_KHLV_KH.html.
24. Omega Engineering, I. *Thermally Conductive Epoxies and Thermally Conductive Grease*. 2009 [cited 2009; Available from: http://www.omega.com/pptst/OB-100_OB-200_OT-200.html.
25. Munson, B.R., D.F. Young, and T.H. Okiishi, *Fundamentals of Fluid Mechanics*. Fifth Edittion ed. 2006, Hoboken, NJ: John Wiley & Sons, Inc.
26. Instruments, N. *NI 9213 16-Channel Thermocouple Input Module*. 2008 [cited 2008; Available from: http://sine.ni.com/nips/cds/view/p/lang/en/nid/208788.
27. Instruments, N. *NI cDAQ-9172 Legacy NI CompactDAQ Chassis*. 2009 [cited 2009; Available from: http://sine.ni.com/nips/cds/view/p/lang/en/nid/202545.
28. Incropera, F.P., et al., *Fundamentals of Heat and Mass Transfer*. Sixth Edition ed. 2007, Hoboken, NJ: John Wiley & Sons, Inc.
29. Bogard, D., *A discussion regarding accurate surface temperature measurement*. 2011.
30. Sinha, A.K., D.G. Bogard, and M.E. Crawford, *Film-cooling Effectiveness Downstream of a Single Row of Holes with Variable Density Ratio.* Journal of Turbomachinery-Transactions of the Asme, 1991. **113**(3): p. 442-449.
31. Technologies, A. *U3401A Digital Multimeter, 4 ½ Digit Dual Display*. 2011 [cited 2011; Available from:

http://www.home.agilent.com/agilent/product.jspx?cc=US&lc=eng&ckey=1650614&nid=-34037.899261.00&id=1650614&pselect=SR.GENERAL.
32. Omega Engineering, I. *Digital Linear Power Supplies*. 2009 [cited 2009; Available from: http://www.omega.com/pptst/PSU300.html.
33. Bejan, A., *Convection Heat Transfer*. Third Edition ed. 2004, Hoboken, New Jersey: John Wiley & Sons.

Vita

Inyeop "Bosco" Jung was born in Seoul, South Korea on February 1, 1985. He was 17 when he moved to Austin, Texas to continue his education in the United States. Upon successful completion of high school in 2005, he attended The University of Texas at Austin with intention to graduate with Bachelors in Science in Mechanical Engineering. He also has worked at Renault-Samsung Motors as an intern where he gained substantial amount of knowledge in fluids and heat transfer. He had participated in cost-reduction projects and performance testing for prototype cars. He also has done research in school with 3-D CAD modeling where he excels at. He also volunteered as an assistant golf coach at local high school for three years which shows that he has talents not only in academics but also other things. He graduated with B.S. in Mechanical engineering in 2009, and started attending graduate program at The University of Texas at Austin in August of 2009.

Permanent address: Giheung-gu Dongbaek-dong Dongwon RoyalDuke 104-1102, Yongin-City, South Korea

This report is typed by Inyeop Jung